Rochester Institute of Technology
RIT Scholar Works

Theses | Thesis/Dissertation Collections

2-1-1998

# Effects of surface characteristics on flow boiling heat transfer

Paul Spiesman

Follow this and additional works at: http://scholarworks.rit.edu/theses

Recommended Citation
Spiesman, Paul, "Effects of surface characteristics on flow boiling heat transfer" (1998). Thesis. Rochester Institute of Technology. Accessed from

This Thesis is brought to you for free and open access by the Thesis/Dissertation Collections at RIT Scholar Works. It has been accepted for inclusion in Theses by an authorized administrator of RIT Scholar Works. For more information, please contact ritscholarworks@rit.edu.

# EFFECT OF SURFACE CHARACTERISTICS ON FLOW BOILING HEAT TRANSFER

by

Paul H. Spiesman

A Thesis Submitted
in
Partial Fulfillment
of the
Requirements for the

MASTER OF SCIENCE
in
Mechanical Engineering

Approved by:

Thesis Advisor _____
Dr. Satish G. Kandlikar

Professor _____
Dr. Arthur E. Bergles

Professor _____
Dr. Moo Hwan Kim

Professor _____
Dr. Alan H. Nye

Professor _____
Dr. Charles W. Haines
Department Head

DEPARTMENT OF MECHANICAL ENGINEERING
COLLEGE OF ENGINEERING
ROCHESTER INSTITUTE OF TECHNOLOGY

FEBRUARY 1998

## PERMISSION TO REPRODUCE

Thesis Title: "Effect of Surface Characteristics on Flow Boiling Heat Transfer"

I, Paul Spiesman, hereby grant permission to the Wallace Memorial Library of the Rochester Institute of Technology to reproduce my thesis in whole or part. Any reproduction can not be used for commercial use or profit.

FEBRUARY, 1998

## FORWARD

I would like to thank all the following people:

- Dr. Kandlikar, who made this whole thing possible.
- Tom, Jim, and Dave for keeping the headaches to a minimum while working in the shop.
- My family for keeping me sane throughout the past few years.
- Karyn for just being there.

## ABSTRACT

The present study focuses on examining the effect of surface characteristics on flow boiling heat transfer by obtaining experimental data for flow boiling of subcooled water over heater surfaces with different surface treatments. Four surfaces with average roughness values of 0.188, 0.363, 0.716 and 3.064 μm, and a commercially prepared sintered surface are employed in a flow boiling setup using water at atmospheric pressure. The apparatus consists of a 9.5 mm circular heater placed on the lower wall of a 3 mm x 40 mm horizontal channel. The results show that surface characteristics can influence heat transfer and are responsible for the scatter in flow boiling data. Cavity geometry seems to be a more important parameter. Only large differences in surface characteristics, such as a sintered surface, produce large increases in heat transfer. A microscope and an imaging software program are used to obtain the cavity distributions for each of the roughened surfaces. The cavity distributions on the surfaces are looked at in light of their experimentally determined heat transfer performance. The differences in the data sets for the four roughened surfaces are in the range of 0% to 28.8%. This comparable to the scatter observed in the flow boiling data from different investigators for experiments conducted under otherwise similar conditions. A discussion is then presented on the possible mechanisms responsible for the enhanced heat transfer due to surface characteristics.

# TABLE OF CONTENTS

## LIST OF FIGURES

## LIST OF TABLES

## NOMENCLATURE

| | | |
|---|---|---|
| $A$ | surface area | $m^2$ |
| $d$ | tube diameter | m |
| $d_H$ | hydraulic diameter | m |
| $i_{fg}$ | heat of fusion | kJ/kg |
| $n$ | number or cavities | - |
| $p_g$ | pressure in the vapor phase | Pa |
| $p_l$ | pressure due to liquid | Pa |
| $q$ | heat flux | $W/m^2$ |
| $r$ | bubble radius | m |
| $r_c$ | cavity radius | m |
| $r_c^*$ | non-dimensional cavity radius | - |
| Re | Reynolds number, $\rho v d_H/\mu$ | - |
| $\Delta T_{sat}$ | $T_{wall}-T_{sat}$ | K |
| $\Delta T^*_{sat}$ | non-dimensional $\Delta T_{sat}$ , see eq. (2.9) | - |
| $\Delta T_{sub}$ | $T_{sat}-T_{bulk}$ | K |
| $\Delta T^*_{sub}$ | non-dimensional $\Delta T_{sub}$ , see eq. (2.10) | - |
| $T_l$ | liquid temperature | K |
| $T_w$ | wall temperature | K |
| $v$ | fluid velocity | m/s |

## Greek Symbols

| | | |
|---|---|---|
| $\alpha$ | single phase heat transfer coefficient | $W/m^2K$ |
| $\delta_t$ | thermal boundary layer thickness | m |
| $\lambda_l$ | conduction coefficient | W/m K |
| $\mu$ | kinematic viscosity | $Ns/m^2$ |
| $\rho$ | density | $kg/m^3$ |
| $\nu$ | specific volume | $m^3/kg$ |
| $\sigma$ | surface tension | N/m |

## Subscripts

| | |
|---|---|
| c | cavity |
| g | vapor |
| l | liquid |
| t | thermal |
| w | wall |

# 1. INTRODUCTION

Both pool boiling and flow boiling heat transfer consist of the convective and nucleate boiling components. It is well established that the pool boiling heat transfer depends strongly on the surface characteristics of the heater surface, such as the size, shape, and distribution of the nucleation cavities. This surface dependence has allowed the development of high performance surfaces. These surfaces utilize artificial cavities from sintered or specially fabricated surface geometries.

It is expected that the nucleate boiling component in flow boiling would show similarities to the pool boiling characteristics, which exhibit the strong surface effect. The flow boiling studies reported in literature have focused on the commercially available plain tubes or tubes with regular fins, microfins, and similar enhancements. The enhancement seen in the nucleate boiling component with microfin surfaces points toward the possibility of surface effects altering the nucleate boiling mechanism and heat transfer (Kandlikar and Howell, 1996, and Kandlikar and Raykoff, 1997).

In the past there has been a certain amount of scatter in flow boiling data for seemingly similar conditions. It is expected that the surface characteristics may be somewhat responsible for this scatter. Since the nucleate component of flow boiling tends to dominate the overall heat transfer mechanism in many cases, it is important that anything affecting it is understood well.

The more this mechanism is understood, the easier it will become to design efficient industrial equipment. Work in this area could prove very important for the heat exchanger, boiler and reboiler, and nuclear power industries. Greater efficiency will come with better heat transfer performance. A surface is considered to perform well if it can transfer a high heat flux at a low wall superheat. Generally that means that the onset of nucleate boiling has taken place at a low wall superheat.

# 2. REVIEW OF LITERATURE

## 2.1 POOL BOILING ENHANCEMENT

As early as 1931, Jakob and Fritz were investigating the effect of surface finish on the pool boiling curve. They used both a sandblasted surface and a surface of 0.016 mm square machined grooves spaced at 0.48 mm. Both of these surfaces showed improved boiling performance, however, the improvement disappeared within a few days. Corty and Foust (1955) reported their work with grit roughened surfaces. This work also showed a decrease in performance with time. Kurihari and Myers (1960) worked with organic fluids boiling on roughened copper surfaces. Figure 2.1 shows their data. They showed that boiling performance was related to the density of active nucleation sites, (n/A), and obtained a correlation showing $\alpha \propto (n/A)^{0.43}$, where $\alpha$ (sometimes known as h) is the overall heat transfer coefficient. Berenson (1962) obtained a 600% increase when boiling pentane on a lapped copper surface. Marto et al. (1968) presented results showing the effects of surface roughness on the pool boiling heat transfer with liquid nitrogen. Surfaces with mirror finish, and mirror finish with various size cavities drilled were tested. Some of their results are shown in Figure 2.2. In general, the surfaces with the cavities exhibited a better heat transfer performance over just the mirror finish surface. All of these works lead to one conclusion. Varying the surface finish changes

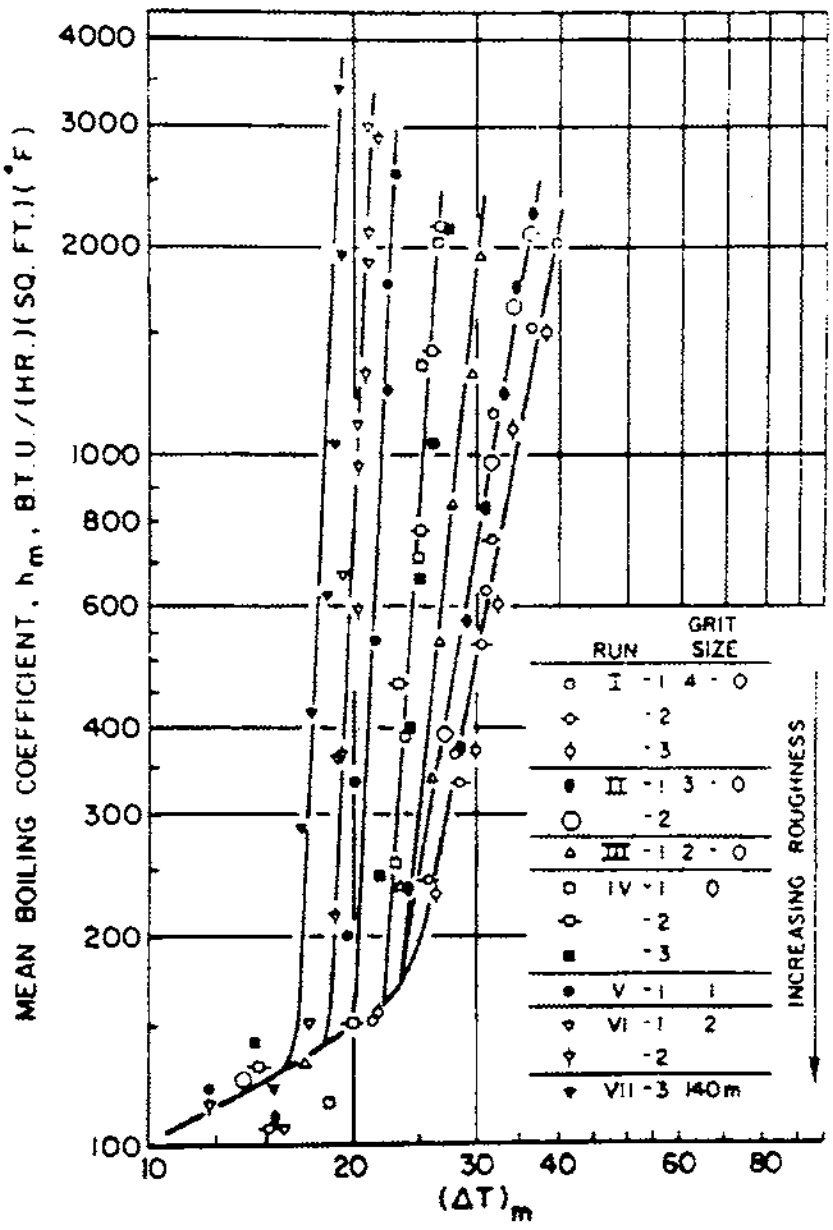


Figure 2.1 Kurihari and Myers work with roughened copper surfaces

Adopted from Webb (1981)

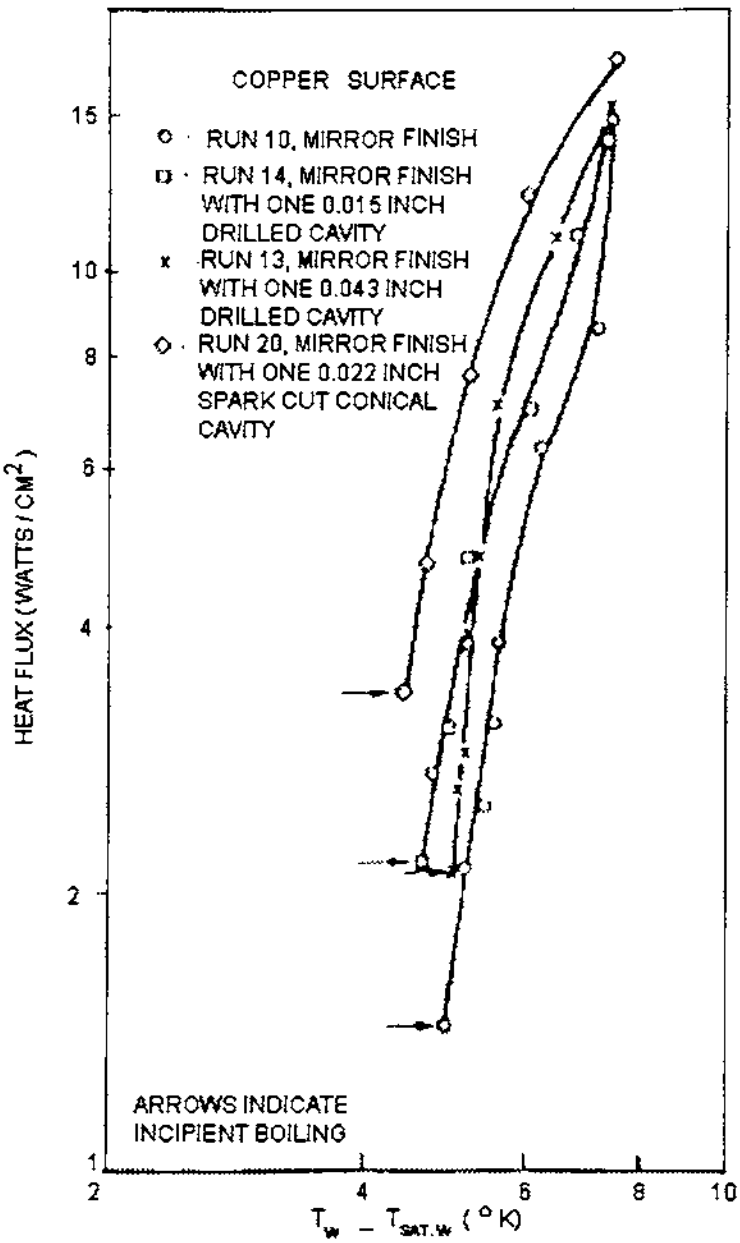


Figure 2.2 Cavity size effects on boiling nitrogen

Adopted from Marto et al. (1968)

the cavity sizes and their distribution and thus directly affects the number of active cavity sites.

By 1971, Gottzmann and O'neil were working with a High Flux copper sintered surface. They determined that the reasons for enhancement were due to the following. First, the porous structure of the surface trapped more vapor-liquid interfaces with large radii. This would require much less wall superheat for nucleation. Second, they concluded that a porous structure such as the High Flux surface would have a greater surface area. This would allow greater evaporation rates. Figure 2.3 is a sample of Gottzmann and O'neil's data for the high flux surface.

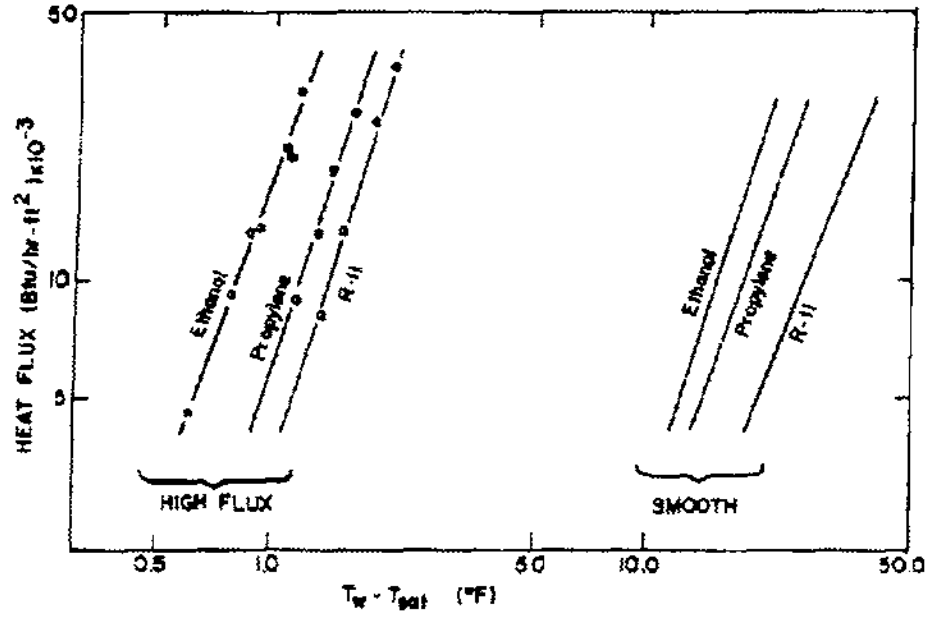


Figure 2.3 Boiling enhancement from High Flux surface

Adopted from Webb (1981)

## 2.2 FLOW BOILING ENHANCEMENT

All of the studies in the previous section dealt with pool boiling. There is not as much in the literature that deals with enhancement during flow boiling due to surface characteristics.

Kandlikar and Howell (1996) examined the effect of microfin surfaces on flow boiling. Their results showed enhancement on the microfin surface. They also reported an increase in bubble activity on the microfin surface when compared to the plain surface. Howell (1996) also reported the effects of surface finish in a flow boiling setup similar to the one used in the present investigation. Average cavity sizes were determined and the conclusion was drawn that the rougher the surface, the lower the required wall superheat is to achieve nucleation. Howell also tested a sintered surface but the results were unclear due to a poor sintering process. This work did lead to the conclusion, however, that surface characteristics might have an effect on the flow boiling heat transfer.

Wadekar (1996) reported an order of magnitude enhancement of flow boiling heat transfer with a commercial UOP High Flux tube using refrigerant R-113. A porous coating of thickness 0.2 mm to 0.3 mm prepared with particle sizes of less than 150 microns (59% less than 44 microns) was used. The Wadekar data is presented in Figure 2.4. It can be seen from the figure that the same heat flux can be obtained with the High Flux surface at much lower wall superheats than with the plain surface. Wadekar postulated in his work that the boiling front in a High Flux tube can move upstream due to the interconnected passages. The

passages allow for the movement of superheated vapor. A plain surface without these passages would have no way of transporting the vapor and therefore could not have any movement of the boiling front without an external change to the system.

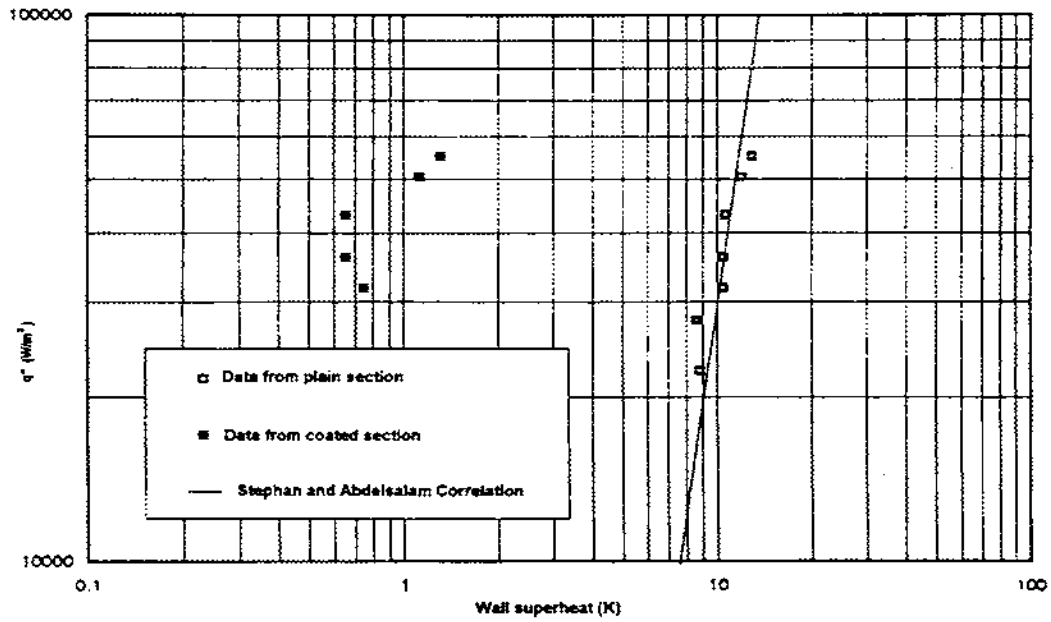


Figure 2.4 Wadekar's High Flux Flow boiling data

Adopted from Wadekar (1996)

Kandlikar, Cartwright and Mizo (1995) used a high speed camera with a microscope to determine nucleating bubble characteristics. They compared their experimentally determined cavity sizes to those determined by the nucleation criteria equations, outlined in the next section. Their results showed that nucleation can be increased by varying conditions such as flow rate, degree of

subcooling and degree of wall superheat. They explained that by increasing wall superheat, the active cavities shifted towards those cavities with smaller radii. The results obtained were consistent with what was expected by the nucleation criteria. This work also leads to the conclusion that surface characteristics can be very important in determining the heat transfer qualities of a surface.

## 2.3 NUCLEATION CRITERIA

The range of active cavity sizes under a given set of conditions is obtained through a nucleation criterion originally proposed by Hsu (1962). The work was then continued by Bergles and Rohsenow (1964) and by Sato and Matsumura (1964). The derivation as it is known today is presented here.

By using the Helmholtz relation, the excess pressure inside a bubble of radius r is given by the differences in the pressure due to the gas and the pressure due to the liquid

$$p_g - p_l = 2\sigma / r \qquad (2.1)$$

where $\sigma$ is the surface tension, and assuming a linear variation, the liquid temperature distribution, $T_l$, in the thermal boundary layer of thickness $\delta_t$ is given by

$$T_l = T_w - \frac{y}{\delta_t}(T_w - T_b) \qquad (2.2)$$

where $T_b$ and $T_w$ are the temperatures of the bulk fluid and the wall, respectively. The Clausius-Clapeyron equation gives the saturation temperature in the bubble

$$\frac{dP}{dT} = \frac{i_{fg}}{T(v_g - v_f)} \qquad (2.3)$$

where $v$ is specific volume of the gas and the fluid and $i_{fg}$ is the heat of fusion of the gas, and at $T_{sat}$ can be written as

$$\frac{dP}{dT} = \frac{i_{fg}}{T_{sat} v_g} \qquad (2.4)$$

when the assumption that $v_g >> v_f$ is made. This is a reasonable assumption in the region away from the critical state. Now from equation 2.4, we obtain

$$\frac{P_g - P_l}{T_g - T_{sat}} = \frac{i_{fg}}{T_{sat} v_g} \qquad (2.5)$$

and when this equation 2.5 is combined with equation 2.1, we get

$$T_g = T_{sat} + \frac{2\sigma}{r} \frac{T_{sat} v_g}{i_{fg}} \qquad (2.6)$$

The condition for a bubble to grow on a given cavity is then obtained by equating the liquid temperature at the bubble top surface (equation 2.2 at y = r) with the saturation temperature inside the bubble (equation 2.6). The range of active cavities is obtained by solving the resulting quadratic equation and the following result is obtained.

$$r_{max}, r_{min} = \frac{\delta_t}{2}\left[\frac{\Delta T_{sat}}{\Delta T_{sat}+\Delta T_{sub}} \pm \sqrt{\left(\frac{\Delta T_{sat}}{\Delta T_{sat}+\Delta T_{sub}}\right)^2 - \frac{8\sigma T_{sat}\upsilon_{lv}}{i_{fg}\delta_t(\Delta T_{sat}+\Delta T_{sub})}}\right] \quad (2.7)$$

Wall superheat is defined as $\Delta T_{sat} = T_w - T_{sat}$ and the localized liquid subcooling is defined as $\Delta T_{sub} = T_{sat} - T_l$. The boundary layer thickness $\delta_t$ can be calculated approximately as $\delta_t = \lambda_l/\alpha_l$ where $\alpha_l$ is the convective heat transfer coefficient from the surface to the liquid calculated by $\alpha_l = q / (\Delta T_{sat} + \Delta T_{sub})$, $\lambda_l$ is the thermal conduction coefficient and q is the heat flux.

By varying some of the parameters in equation 2.7, a variety of plots such as Figure 2.5 can be obtained for comparative purposes. Figure 2.5 shows the effects of varying the single phase convection coefficient. This would correspond to a change in flow rate during flow boiling. As flow rate is increased, so is the single phase heat transfer. This forces only the smaller cavities to nucleate and delays the onset of nucleate boiling. The effects can become quite substantial as can be seen at $\alpha_l$=50,000 W/m$^2$K, where ONB is delayed until the wall superheat reaches a value of 9.7K.

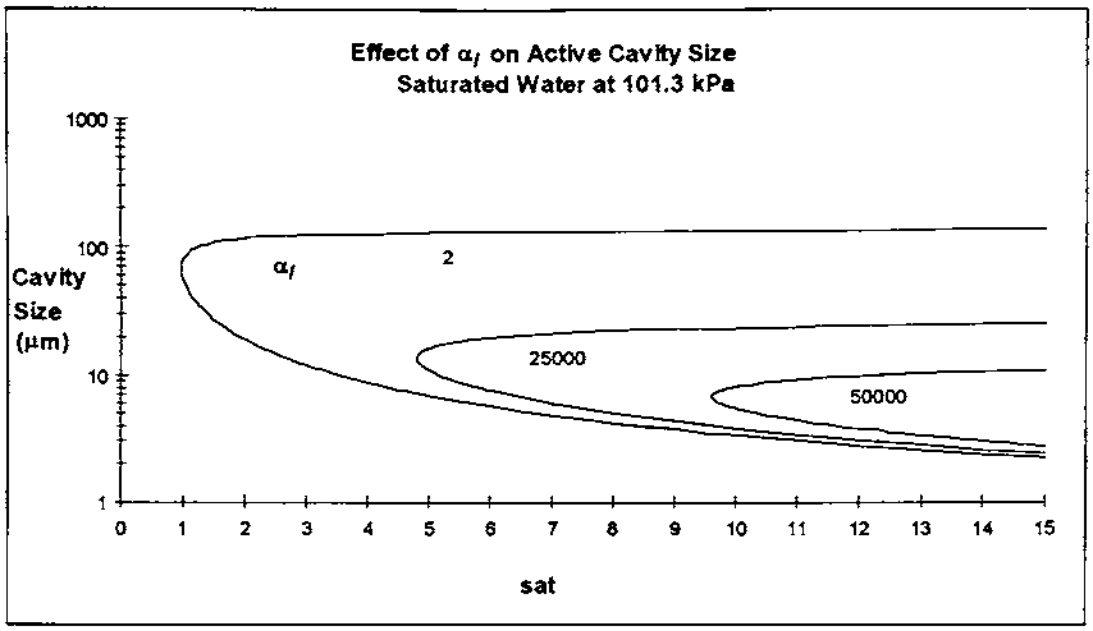


Figure 2.5 Effect of flow rate on cavity range for saturated liquid in flow boiling

Adopted from Kandlikar and Spiesman (1997)

Equation 2.7 gives the range of active cavity sizes for specific flow conditions. Kandlikar and Spiesman (1997) non-dimensionalized this equation in order to compare the nucleation criteria under different conditions. The non-dimensional form is derived here.

Three non-dimensional quantities $r_c^*$, $\Delta T^*_{sat}$, and $\Delta T^*_{sub}$ are defined.

$$r_c^* = r_c/\delta_t \qquad (2.8)$$

$$\Delta T^*_{sat} = \Delta T_{sat} i f g \delta_t/(8 s T_{sat} \qquad (2.9)$$

$$\Delta T^{*}_{sub} = \Delta T_{sub} i f g \delta / (\sigma T_{sat} v_{lv}) \qquad (2.10)$$

Introducing the above non-dimensional parameters in equation 2.7, the following non-dimensional form for active cavity range is obtained as equation 2.11.

$$r^{*}_{max}, r^{*}_{min} = \frac{1}{2}\left[\frac{\Delta T^{*}_{sat}}{\Delta T^{*}_{sat} + \Delta T^{*}_{sub}} \pm \sqrt{\left(\frac{\Delta T^{*}_{sat}}{\Delta T^{*}_{sat} + \Delta T^{*}_{sub}}\right)^{2} - \frac{1}{(\Delta T^{*}_{sat} + \Delta T^{*}_{sub})}}\right] \qquad (2.11)$$

Figure 2.6 shows the non-dimensional cavity sizes with non-dimensional subcooling as a parameter. It can be seen from Figure 2.6 that with increasing subcooling, the range of active cavity sizes is decreased. The wall superheat required is also less to produce the first nucleation. At $\Delta T^{*}_{sub}$=0, corresponding to the saturation condition, ONB occurs in cavities with the radii equal to half the boundary layer thickness. Also when the liquid is saturated, the maximum value of $r_c^{*}$ approaches 1 as $\Delta T^{*}_{sat}$ is increased. This corresponds to maximum active cavity radius equal to the boundary layer thickness. This non-dimensional plot can be used in designing and comparing the performance of a surface with different fluids under different operating conditions.

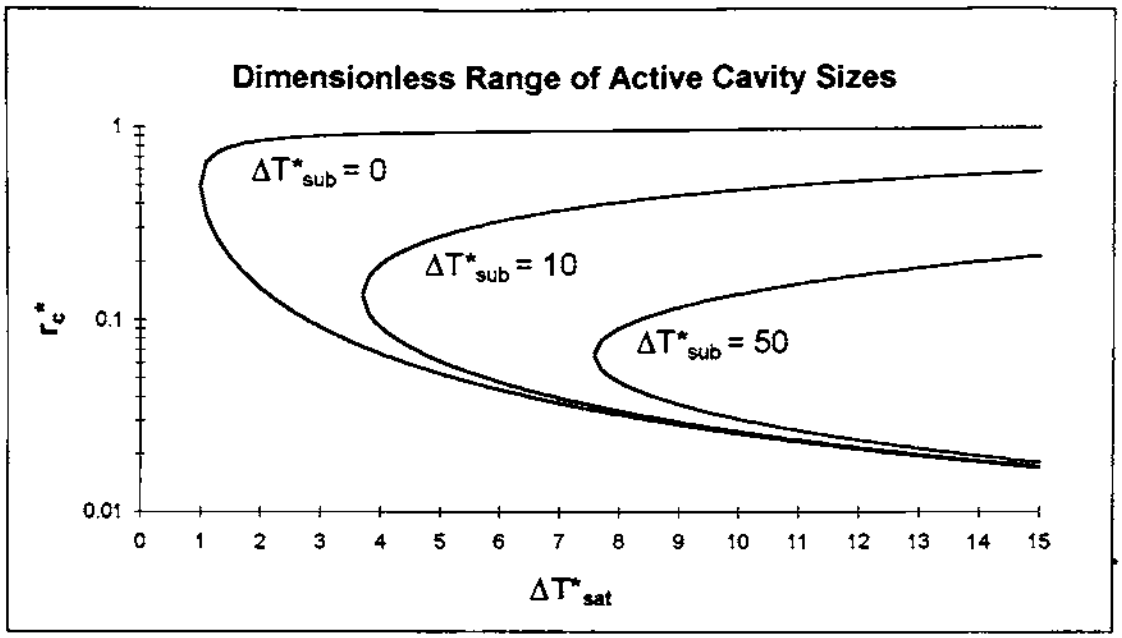


Figure 2.6 Non-dimensional representation of active cavity range

Adopted from Kandlikar and Spiesman (1997)

The effect of surface roughness on flow boiling heat transfer was further analyzed by Kandlikar and Spiesman (1997) by comparing the active cavity range with the available cavity range satisfying the nucleation criteria. Figure 2.7 shows their qualitative plot of the cavity size distribution for two different surfaces I and II. Depending on the fluid and the operating conditions, the range of active cavities could cover different regions of the available cavity ranges.

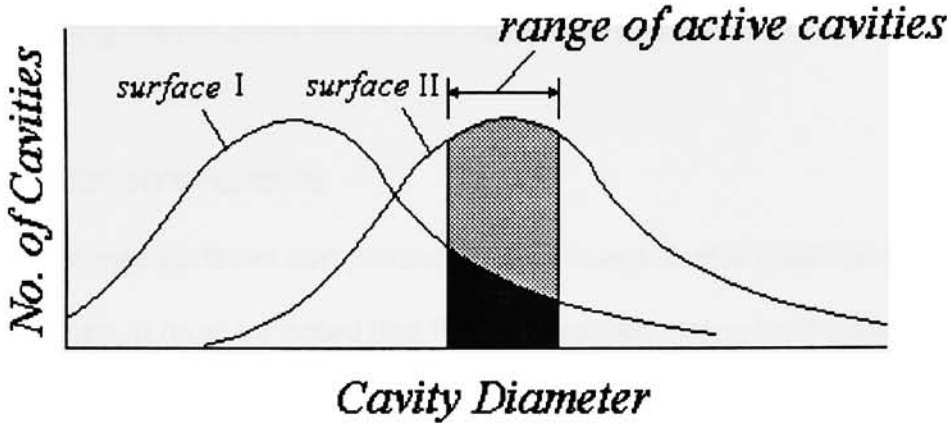


Figure 2.7 Cavity Distributions

Adopted from Kandlikar and Spiesman (1997)

For the active cavity range shown in Figure 2.7, surface II will yield a higher heat transfer as a greater number of cavities are able to nucleate. However, if the active cavity range shifts to the left, surface I is expected to perform better. The polishing process using sandpaper of different grit sizes would yield different cavity size distributions. The resulting cavity size distribution and the actual operating conditions will be the governing factors in the thermal performance of a given surface. This information can be utilized in developing optimized sintered surfaces for flow boiling applications. It must be remembered that Figure 2.7 is a schematic plot. The cavity distributions are shown as near perfect bell curves. In actuality, the cavity distribution may look nothing like this. The figure is just used to illustrate the point that the cavity distribution will affect

the number of active cavities and thus the heat transfer from the surface. More realistic cavity distributions will be discussed in a later section.

## 2.4 NOTE ON HYSTERESIS

While sintered surfaces can produce higher heat transfer coefficients than plain surfaces, it must be noted that they can exhibit strong hysteresis effect. The hysteresis effect starts when certain cavities are activated as nucleation sites at high wall superheats. As the wall superheat is then decreased, these active cavities continue to produce bubbles at lower superheats than they normally would. With these added nucleation sites comes an enhancement in heat transfer. This may or may not be a problem but it must at least be recognized as it will dramatically affect the heat transfer. Any surface can demonstrate hysteresis effects but the sintered surfaces seem to be most pronounced. This could be because they have such a large number of cavities available to begin with. Figure 2.8 is an example of hysteresis that was found experimentally by Marto et. al. (1968). The graph shows how the same experimental heat transfer values were not obtained when increasing and decreasing the heat flux. They attributed the additional activated cavities due to the spreading of boiling patches. Hysteresis has been observed by many other researchers and can be considered quite common.

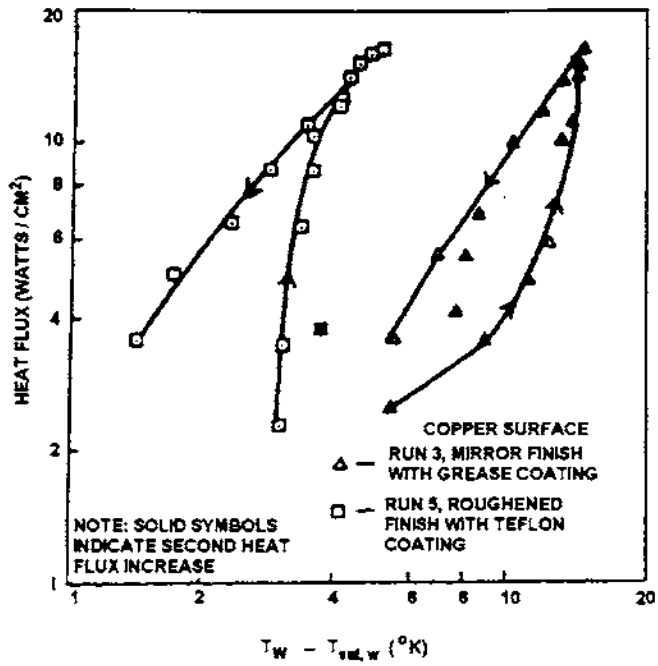


Figure 2.8 Effects of hysteresis

Adopted from Marto et. al. (1968)

## 2.5 PORE CLASSIFICATION

Cavities on a boiling surface are often referred to as "pores." Many authors have classified these pores into different categories. One such classification is outlined in this section. Although no classification system should be considered correct or incorrect, the Czikk and O'Neil model (1979) seems to be one of the better models due to its simplicity. They break down all the cavities or pores into four categories. These four categories are: 1. Active pores, 2. Intermittent pores, 3. Liquid-filled pores, and 4. Non-functional pores. Active pores are

classified as those that always contain vapor bubbles. These pores are the re-entrant type which means they are able to trap the vapor and can be considered stable nucleation sites. The intermittent pores are non re-entrant cavities that contain vapor that has traveled from the active pores through passages connecting them. They will nucleate bubbles but could not do so without the vapor from the active pores. The liquid-filled pores are similar to the intermittent pores in they are both connected to active pores. These liquid-filled pores are the sites where the liquid becomes superheated before being passed on to the active pores. Finally, the nonfunctional pores are those that are sealed off from the liquid in some way and are not wetted.

All of the research presented in this section has shown how surface structure can affect nucleation, boiling, and heat transfer. In general, it has been determined that the rougher the surface, the more heat it will be able to transfer. In light of all of the works, it seems like cavity size and distribution could be a valid parameter for determining how well a surface will perform.

## 3. OBJECTIVES OF THE PRESENT WORK

The present study has the following objectives:

- Obtain experimental data for flow boiling heat transfer of subcooled water at atmospheric conditions over heater surfaces of four different surface treatments. The heater consists of a 9.5 mm circular heater placed on the lower wall of a 3 mm x 40 mm horizontal channel.
- Obtain experimental data for flow boiling heat transfer of subcooled water over a commercially prepared sintered surface in the same test setup. Hysteresis effects will also be tested on this sintered surface.
- Analyze the surfaces using a surface roughness tool as well as a software imaging program. With these tools, obtain a cavity size distribution for each of the four roughened surfaces.
- Compare the cavity distributions of the surfaces to the relative heat transfer characteristics they produce.
- Present a discussion on the mechanisms governing the effect of surface characteristics on the nucleate portion of flow boiling heat transfer.

# 4. EXPERIMENTAL APPARATUS AND TEST PROCEDURE

## 4.1 EXPERIMENTAL SETUP

The experimental setup that was used was very similar to that of Kandlikar and Howell (1996) and also Raykoff (1996). Slight modifications were made to improve the flow loop and to allow for easier data collection. The system is designed to simulate flow boiling at various conditions and collect data during the process. A pictorial representation of the experimental setup can be seen in Figure 4.1.

### Test Section

The test section was a 3mm x 40mm rectangular flow channel approximately 400mm in length fabricated from 2024-T3 aluminum. It was equipped with a two piece polycarbonate window above the heater to allow for viewing through a microscope as well as taking video. A torlon bushing was used to hold the heater in the test section as well as insulate the heater from the test section. Atmospheric pressure was maintained in the test section by the flow control valves located at the inlet and the outlet of the flow loop.

### Heater

The heater was machined out of 6061-T6 aluminum. It contained thermocouples along the length of the 9.5 mm rod. A constant heat flux was

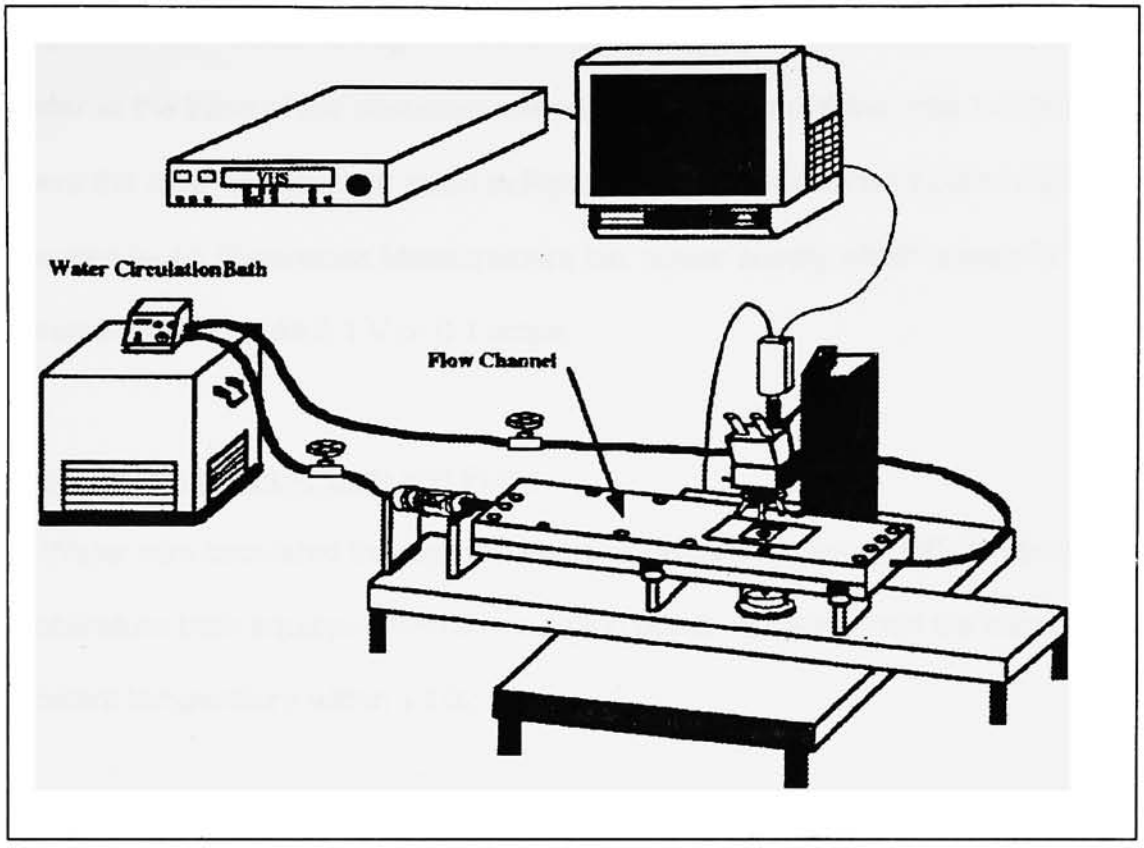


Figure 4.1 Pictorial Representation of Experimental Setup

Adopted from Stumm (1995)

supplied to the heater through a Watlow circumferencial electrical resistance heater at the base of the aluminum element. A schematic of the area in the setup where the data was taken is given in Figure 4.2. The resistance heater was powered by an Electronics Measurement Inc. power supply which allows for increments as little as 0.1 V or 0.1 amps.

Constant Temperature Bath and Pump

Water was circulated through the test section by a Brinkman RC-20 constant temperature bath equipped with a circulation pump. It maintained the water at a constant temperature within ±0.02 K.

Thermocouples and Thermocouple Scanner

Four E type thermocouples were used spaced along the length of the heater and one was used in the test section, just downstream of the flow. Figure 4.3 shows greater details of the heater and the spacing of the thermocouples. The thermocouples were connected to a digital Keithley 740 System Scanning Thermometer that displayed the various thermocouple readings. The temperature readings had a precision of 0.1°C.

Flowmeter

The flow rate was monitored by an Omega FL-1503A rotameter with a maximum flow of 2.53 GPM (gallons per minute). The flowmeter had a precision of 0.0253 GPM.

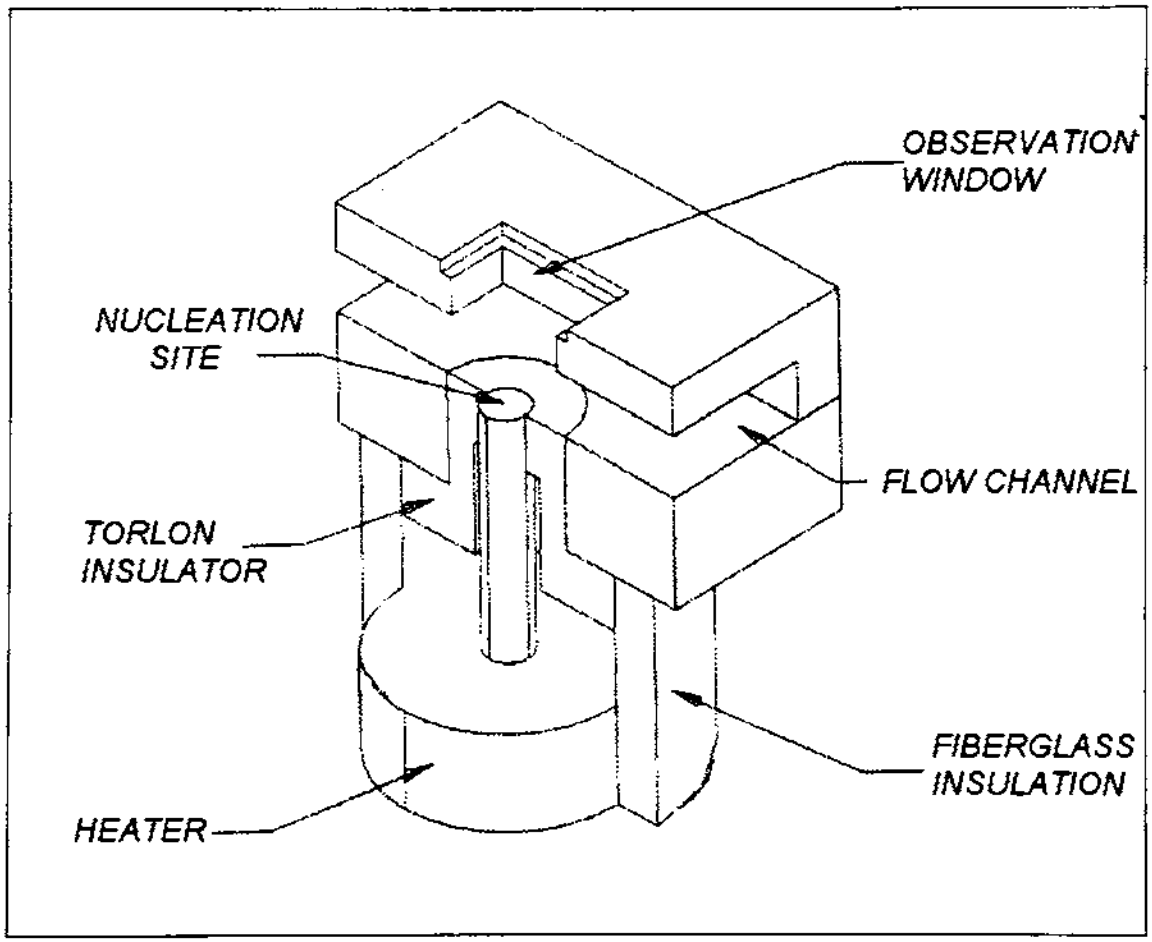


Figure 4.2 Region of data acquisition

Adopted from Howell (1996)

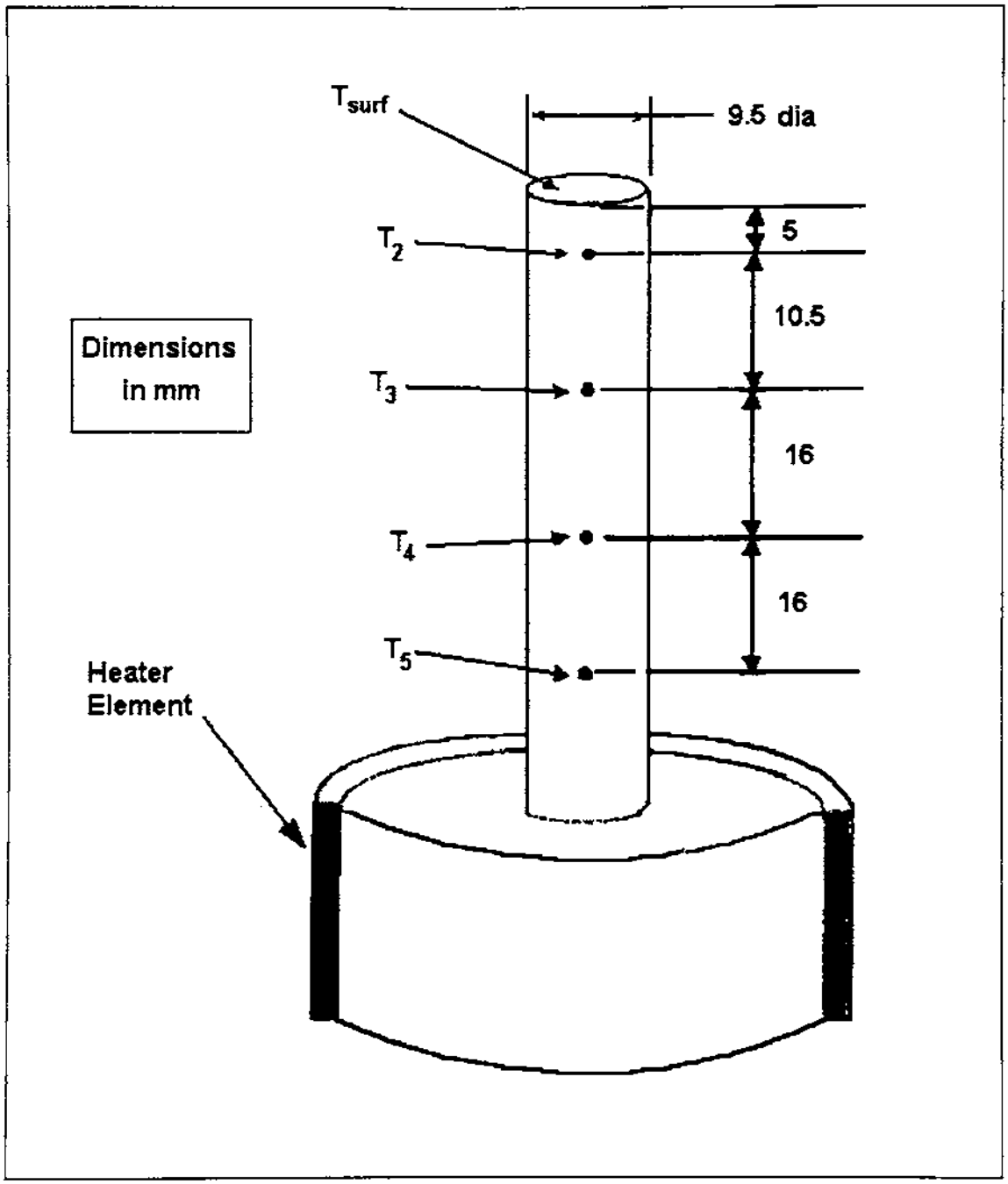


Figure 4.3 Heater detail and spacing of thermocouples

Adopted from Raykoff (1996)

Microscope and Camera

A Mitutoyo WF microscope consisting of 3 various magnification objective lenses was used in the analysis of the heater surfaces. Attached to the microscope was a Hitachi KP-C501 solid state camera. This camera was directly connected to a PC that was loaded with Image-Pro PLUS™ software. The whole imaging system allowed for magnifications of 125X, 250X, and 500X. Once the image was captured on the PC, it could then be saved for future analysis.

## 4.2 TEST PROCEDURE

Preparation of Surfaces

The heater surfaces were prepared as follows. First the heater surface was polished with 400 grit Wet-Dry Silicon Carbide grinding paper. This surface was then analyzed and tested. Then the 600 grit was used and again the surface was analyzed and tested. The same heater was used to minimize error in the heat transfer calculations. By doing so, the thermocouple locations are known to be in the exact same spot and any material variations in the heater will not become an issue. The third surface tested was then polished with a 1 μm silica solution and then with the 0.03 μm silica solution to give it a mirror like finish. The fourth surface tested was then roughened with 120 grit paper to give a very rough finish. Table 4.1 shows the surface roughness calculations for the four surfaces that were tested and their respective average roughness values.

Surface roughness was measured with a FEDERAL PocketSurf® I Portable Surface Roughness Gage. Multiple readings were taken on each surface to get an average roughness over the whole surface. The preparation of each surface left inherent scratches in a preferred direction. To deal with this, each of the four surfaces were placed in the flow section so that these scratches were at a 45° angle with the direction of the flow. This made sure there were no variations due to surface structure orientation. Finally, the fifth surface that was tested, the UOP High Flux surface, was optimized for hydrocarbons. It consisted of a 225-300 μm thick layer of sintered particles with a porosity of 40-60%. The effective pore sizes for this surface were not disclosed by the manufacturer. This surface does not appear on the table since the surface roughness was out of the gages range. Also this surface was just tested for comparative purposes and to test for hysteresis.

| Reading # | Surface Preparation | | | |
|---|---|---|---|---|
| | 0.03 μm Solution | 600 Grit | 400 Grit | 120 Grit |
| 1 | 8 | 13 | 25 | 134 |
| 2 | 12 | 24 | 32 | 92 |
| 3 | 6 | 13 | 28 | 148 |
| 4 | 6 | 12 | 22 | 95 |
| 5 | 9 | 15 | 26 | 97 |
| 6 | 6 | 15 | 31 | 140 |
| 7 | 7 | 11 | 25 | 103 |
| 8 | 7 | 13 | 36 | 92 |
| 9 | 6 | 15 | 30 | 152 |
| 10 | 7 | 12 | 27 | 143 |
| 11 | - | - | - | 131 |
| Average | 7.4 (0.188 μm) | 14.3 (0.363 μm) | 28.2 (0.716 μm) | 120.6 (3.064 μm) |

*All dimensions in μin unless noted

Table 4.1 Surface Roughness Calculations

Surface Analysis

The Image-Pro PLUS™ software simplified the analysis of the surfaces that were tested. After a surface was prepared, images at the three available magnifications were taken. Using a counting feature of the software an approximate count of cavities could be obtained. Since the images obtained were black and white, the cavities were taken to be the darker spots while the brighter spots were assumed to be relative high points on the heater surface. The software was used to measure the average diameter of each dark spot. With this data, an approximate size distribution of cavities could be plotted. Prior to each count, the image was calibrated for the proper magnification. This

was accomplished by placing a slide with tic marks at known spacing under the same magnification and obtaining an image. Then using the software package, the image could be calibrated for that magnification.

Data Acquisition

Before taking any data, the constant temperature water bath was heated to about 98°C. It was then allowed to circulate at this temperature for 3 to 4 hours to ensure that the water was as de-gassed as possible. The bath temperature was then allowed to cool to its desired degree of subcooling and then adjusted to the proper flow rate. The flow rate was adjusted by both changing the pumping rate and by adjusting the two valves connected to the test section. These two valves also regulated the pressure inside the test section. The pressure was set at one atmosphere. The power supply was then turned on which gave a heat flux through the heater. After the whole system reached a steady-state temperature, the first reading was taken. After all pertinent information was recorded, the heat flux was increased through the heater. Appendix B is the data obtained and used in this work. This was done by increasing the voltage across the resistance wrap heater. The voltage was usually raised in 5V increments. This caused an increase of about 0.07 amps in the current through the heater resulting in a 0.35 W increase in power for each step. In the cases where decreasing heat flux were also recorded, the decreasing step size was varied between 2V and 5V.

Data Reduction

From the four thermocouple readings along the length of the heater and the thermal resistance of the heater material, the heat flux through the heater could be determined. Equation 4.1 was used for the calculation of the heat fluxes.

$$q'' = \frac{k}{x} \Delta T \qquad (4.1)$$

The losses between each section of heater were minimal, on the order of 1-2%, so a linear interpolation was used to determine the surface temperature. The surface temperatures obtained in this way were accurate to within 0.1 K of the surface temperature predicted by Thermonet®, a heat transfer software package. Along with the bulk temperature of the fluid, this surface temperature could then used to find the local convection coefficient, $\alpha$, for that surface using equation 4.2.

$$q'' = \alpha \, (T_{surf} - T_{bulk}) \qquad (4.2)$$

The surfaces, however, during comparison were looked at in regards to the heat flux obtained from them. The data reduction was reduced using an Excel spreadsheet.

# 5. RESULTS AND DISCUSSION

The experimental apparatus described in section 4.1 was utilized to study the effect of surface finish of the heater surface on the flow boiling heat transfer. All experiments were conducted with subcooled water at 95 °C at atmospheric pressure. Table 5.1 is a summary of the four surfaces described in table 4.1 along with a fifth sintered surface. The first four surfaces are the focal point of the discussion on surface characteristics and cavity distribution. Surface E-UOP, the sintered surface, will be discussed later in section 5.3 as it relates to the effect of hysteresis.

| Surface | Preparation Method | Average Roughness (μm) |
|---|---|---|
| A-188 | 0.03 mm soluton | 0.188 |
| B-363 | 600 grit | 0.363 |
| C-716 | 400 grit | 0.716 |
| D-3064 | 120 grit | 3.064 |
| E-UOP | UOP High Flux Surface | NA, sintered layer thickness |
| | | 225-300 μm, porosity 40-60% |

Table 5.1 Details of the five surfaces tested

## 5.1 EFFECT OF CAVITY DISTRIBUTION

The procedure outlined in section 4.2 was followed and the results obtained are shown in Figures 5.1 and 5.2. Figure 5.1 is a plot of heat flux (y-axis) vs. wall superheat (x-axis). This figure corresponds to a Reynolds number of 2253.

In the low ranges of wall superheat, up to about 10 degrees, all the surfaces perform about the same, each with a single-phase convective heat transfer coefficient of about 4500 $W/m^2K$. This is expected since this is only convective heat transfer and there is no nucleate boiling component. As wall superheat rises above 10 degrees however, there is a sharp increase in the heat flux obtained. This is the point of the onset of nucleate boiling. Surface D-3064 performs the best followed by surfaces B-363 and A-188. Surface C-716 tends to perform the worst at these flow conditions.

Figure 5.2 is very similar to figure 5.1 except that it corresponds to a Reynolds number of 7163. Again, at low wall superheats in the convective only heat transfer region, the surfaces all perform very much the same. For these runs the single-phase coefficient was higher though, at about 7000 $W/m^2K$. At higher wall super heats, surface D-3064 and surface A-188 perform about the same, slightly better than surfaces B-363 and C-716.

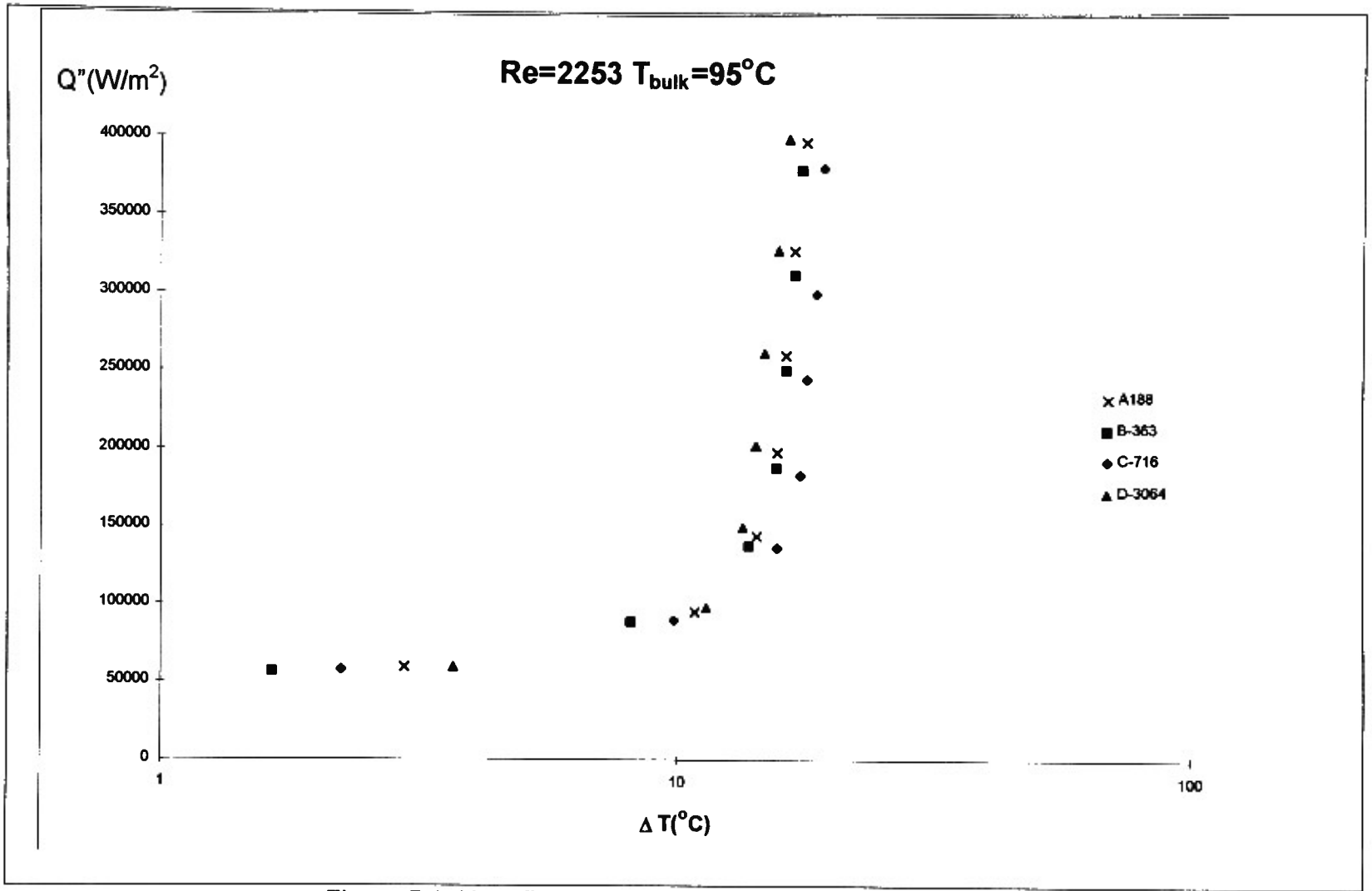


Figure 5.1 Heat flux versus wall superheat results for Re =2253

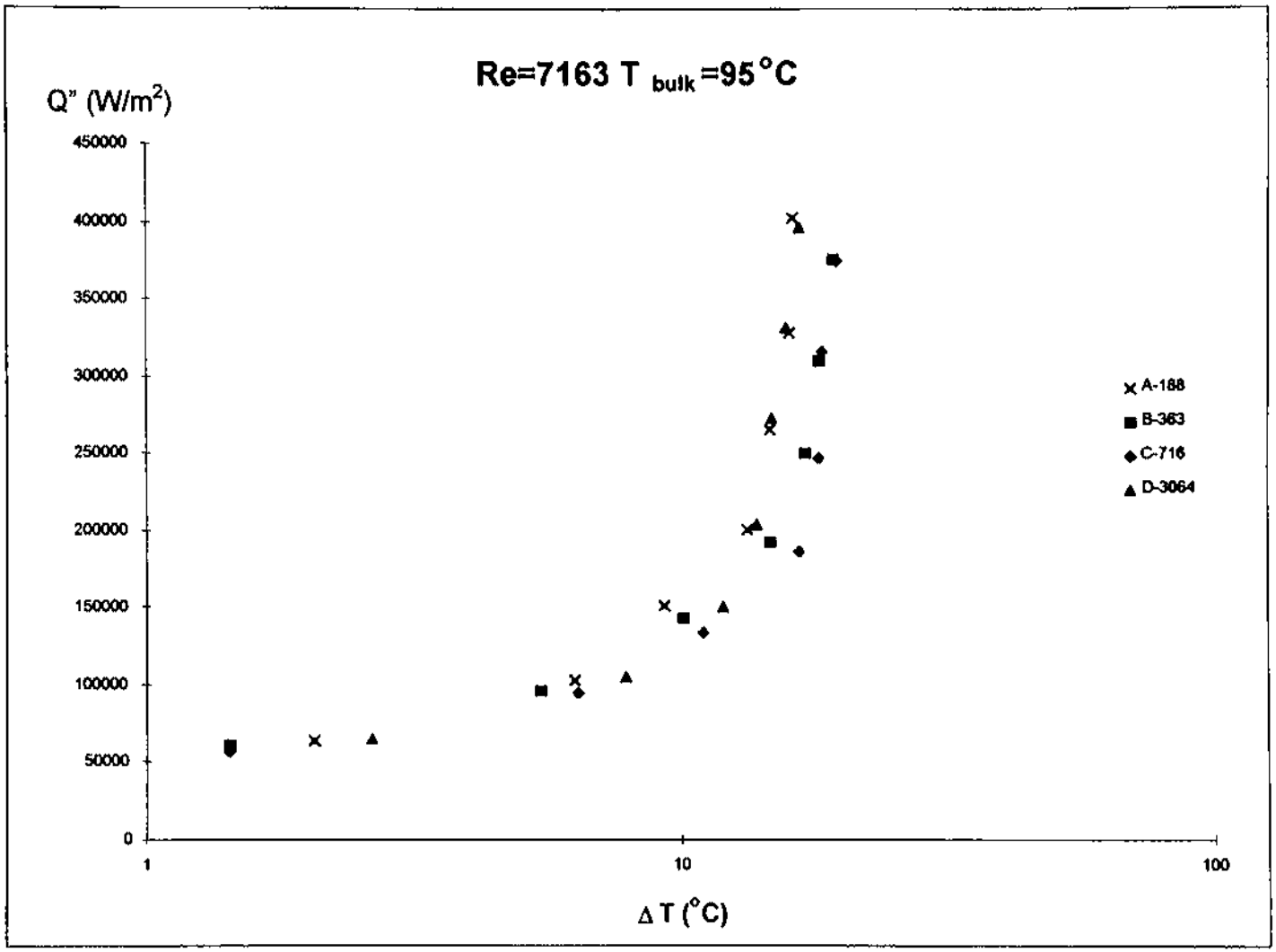


Figure 5.2 Heat flux versus wall superheat results for Re =7163

The heat flux curves in both figures 5.1 and 5.2 vary in degree of wall superheat in the range of 0-28.8% for a given heat flux. It can be seen that no definite conclusion can be drawn from figures 5.1 and 5.2 on the basis on average roughness. It can then be concluded that average surface roughness is not a very good indicator of the performance of a surface. This is because there are many other parameters contributing to the overall heat transfer. Both bubble departure diameter as well as bubble frequency can help to determine the overall heat transfer rate. Average roughness is only one of many parameters that will affect total heat transfer.

Since average surface roughness does not seem to be the main factor governing the heat transfer performance, perhaps the cavity size distribution will provide a better understanding of the heat transfer characteristics for a particular surface. A surface with a large number of large cavities and a large number of small cavities may have an average surface roughness that is not a true representation of its surface characteristics.

The method of determining the range of active cavity sizes using the nucleation criteria was discussed in section 2.3. Table 5.2 was constructed using equation 2.7 and the criteria outlined in that section. The theoretical sizes of cavities that should be able to nucleate are given for various wall superheats at two different Reynolds numbers. From the table, it can be seen that at the low flow rate tested, the onset of nucleate boiling should occur at about 2.6° wall superheat in cavities with diameters of about 51μm. At the higher flow rate

tested, ONB should occur at about 3.4° wall superheat in cavities with diameters of about 39 μm. The rest of the table shows the ranges of theoretical active cavity diameters at varying degrees of wall superheat. Thus, depending on the flow rate, surfaces with different cavity size distributions should have different heat transfer characteristics.

| Theoretical Active Cavity Diameters (all dimensions in μm) | | |
|---|---|---|
| Wall Superheat | Re = 2253 | Re = 7163 |
| 2.6° | ONB 51 | None |
| 3.4° | 24 - 98 | ONB 39 |
| 5° | 14 - 136 | 16 - 82 |
| 10° | 7 - 194 | 7 - 122 |
| 12.5° | 5 - 212 | 5 - 134 |
| 15° | 4 - 222 | 4 - 141 |

Table 5.2 Range of active cavity sizes at flow rates tested

Figures 5.3-5.6 are the cavity size distributions obtained from the imaging software used in the surface analysis. The procedure used to obtain these distributions is outlined in section 4.2. All four of the graphs show cavity diameter in microns vs. number of cavities counted per square mm. The cavities were counted per image by the software and therefore should be looked at relative to each other. These numbers are not totals for the each heater surface as a whole. The sample areas analyzed were 1.08 $mm^2$ while the whole area of the heater is about 70.88 $mm^2$.

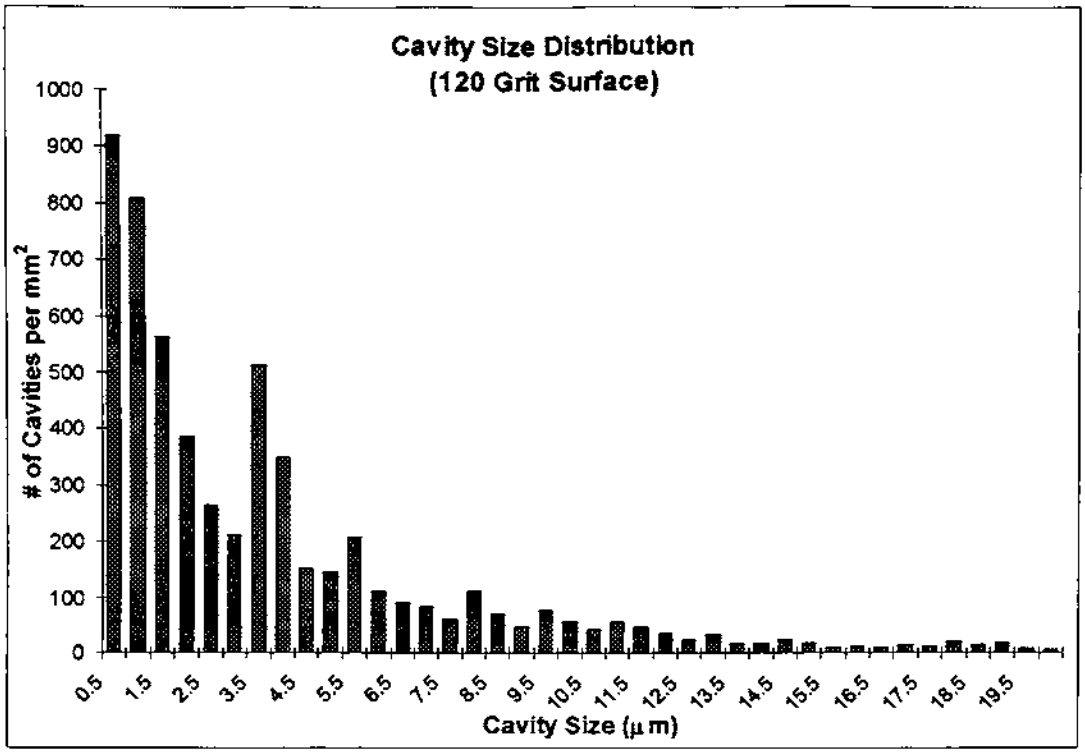


Figure 5.3 Cavity distribution of surface D-3064 with 3.064 μm $R_a$

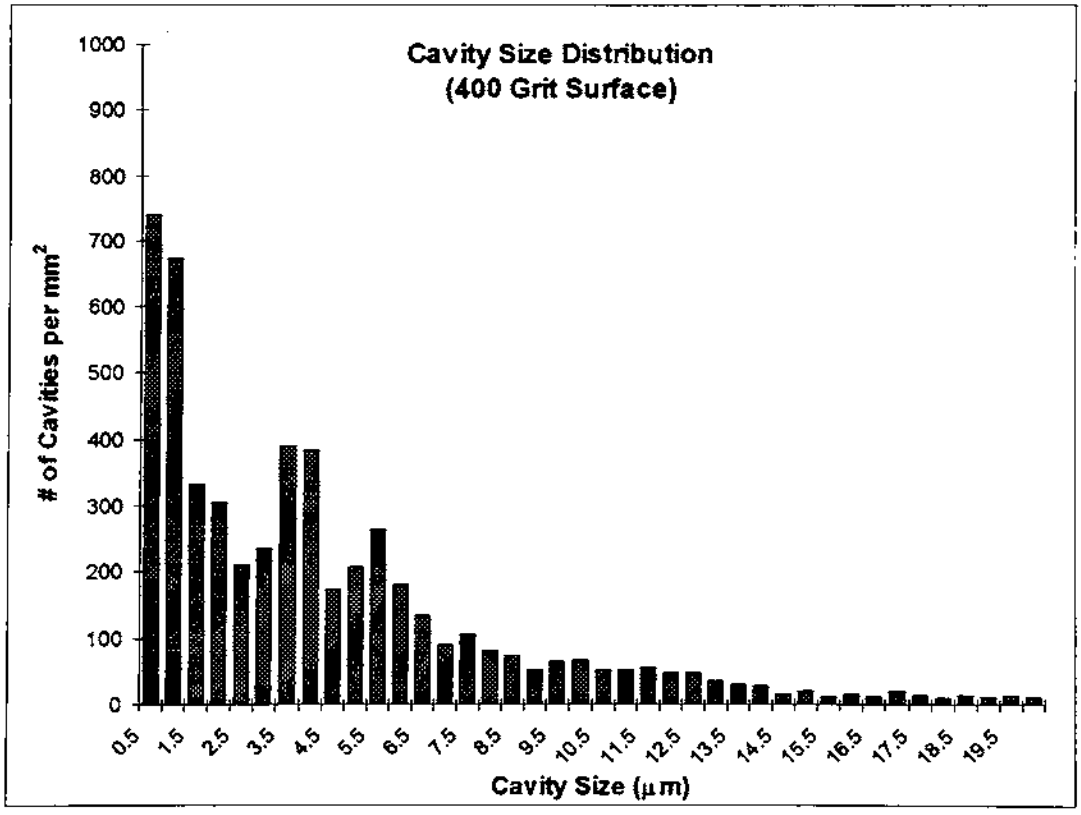


Figure 5.4 Cavity distribution of surface C-716 with 0.716 μm $R_a$

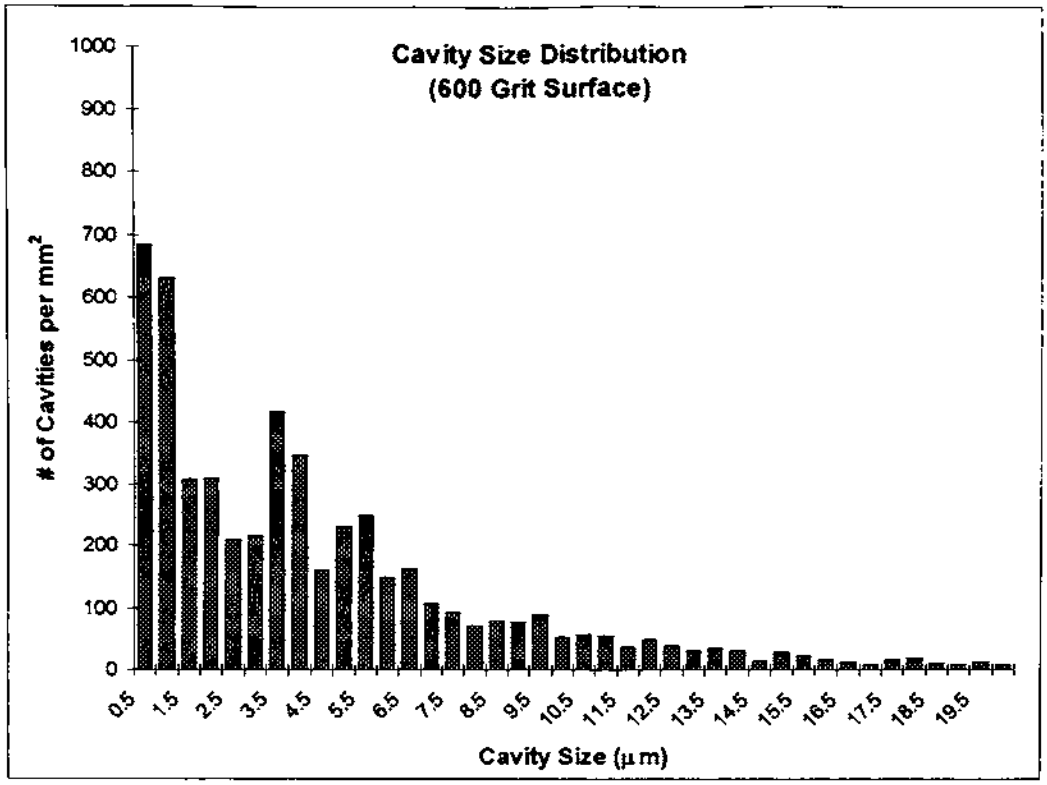


Figure 5.5 Cavity distribution of surface B-363 with 0.363 μm $R_a$

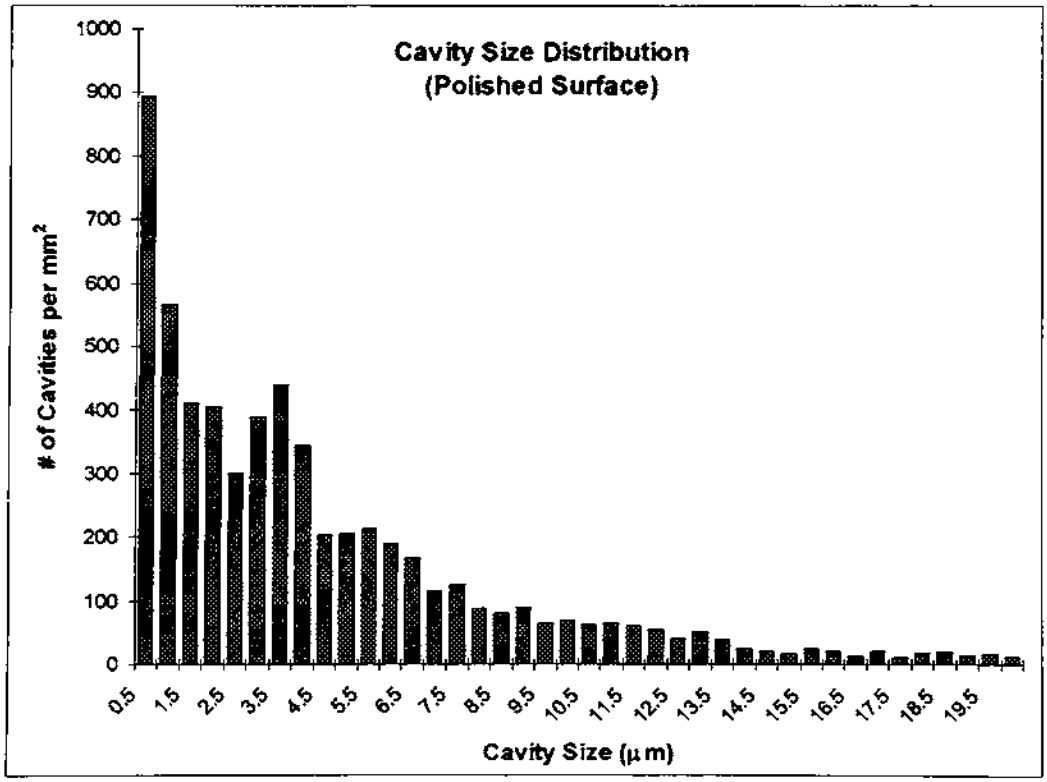


Figure 5.6 Cavity distribution of surface A-188 with 0.188 μm $R_a$

There were many relatively large cavities on each surface also. These cavities were grouped together and are outlined in table 5.3. The total counts of theses cavities with diameters over 20 μm are shown in this table for each figure.

| Surface | 20 μm+ cavities |
|---|---|
| A-188 | 149 |
| B-363 | 162 |
| C-716 | 180 |
| D-3064 | 208 |

Table 5.3 Number of cavities over 20μm per $mm^2$

As table 5.2 shows, cavities of well over 20 μm are in the theoretical range of active cavities. Therefore, the counts in table 5.3 can be considered significant. These cavity size distributions can be very helpful when determining the onset of nucleate boiling.

Combining table 5.2 with the cavity distributions, a surface's performance potential can be seen. This is presented in figure 5.7. All four cavity size distributions are superimposed onto a single plot and the lower bound of theoretical active cavity size at various degrees of wall superheat is shown. The similarities of all the surfaces tested can be seen. This helps to explain the similarities in the heat flux curves in figures 5.1 and 5.2.

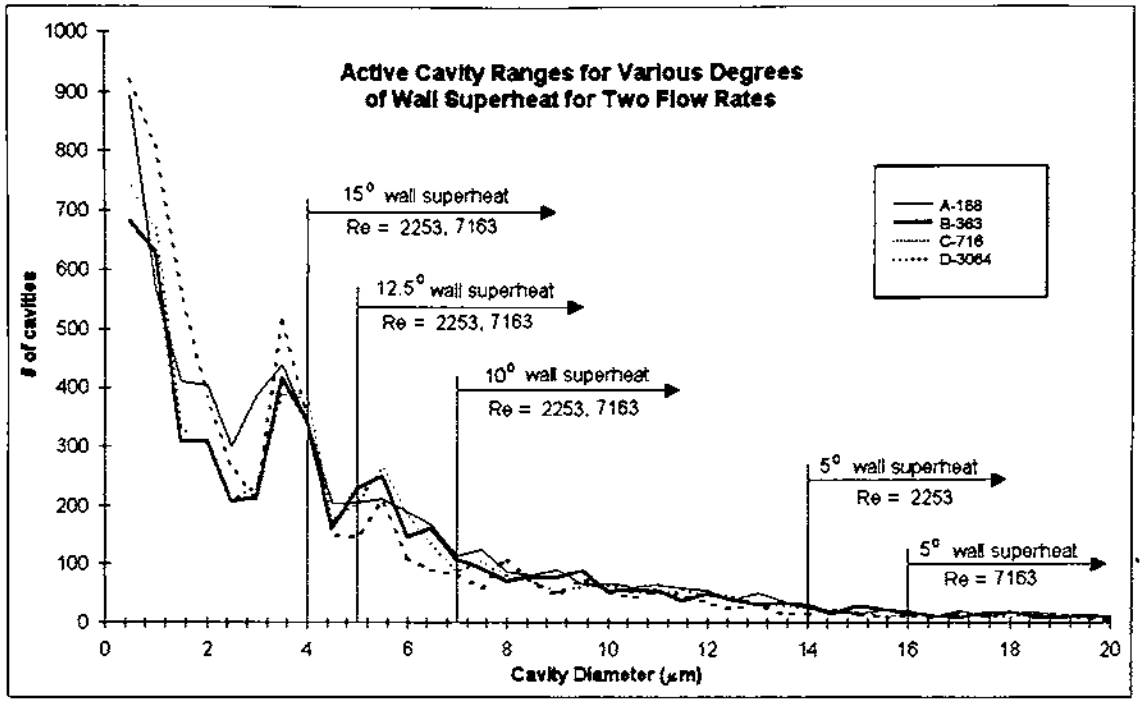


Figure 5.7 Cavity size distribution for 4 different surfaces

As wall superheats increase, the range of active cavities grows to include smaller and smaller cavities. It is recommended that these distributions be used over average surface roughness when determining how a surface will perform. There are many other factors that must be considered as well though. It is expected that cavity structure is a very important parameter in flow boiling heat transfer.

## 5.2 POSSIBLE EXPLANATION FOR SURFACE EFFECT

All surfaces tested are in the range of surface roughness that a manufactured commercial industrial tube would have. Certain experiments in the past have

been known to be hard to reproduce exactly. It is expected that this is due to these surface characteristics. Usually this is just accepted as flow boiling "scatter." From this investigation, the "scatter" was in the range of 0% -28.8%. To obtain any greater enhancement in a commercial tube than this, it is recommended that a more drastic measure such as sintering or artificial cavities be implemented.

Cavity structure of the surfaces may also be a contributing factor. The 400 and 600 grit sandpapers had very similar textures. The 120 grit was very different even though it was the same type of grinding paper. It is very possible that the way these each of these sandpapers works would produce very different types of cavities. If the cavity radius is in the right size range, shape and structure could be the most dominant force affecting the boiling mechanism. The polishing method used is a completely different process than the grinding paper and would also produce different structured cavities. The images in Appendix A support this theory since the rough surface and the polished surface both look drastically different than the two intermediate surfaces which look similar to each other. Figures A.1, A.5, and A.9 are all the roughest surface D-3064. Figures A.2, A.6 and A.10 are all of surface C-716 which look very similar to Figures A.3, A.7 and A.11, respectively, which are all of surface B-363. Surface A-188 which is shown in Figures A.4, A.8, and A.12 looks quite different than all the others. Surface treatments that produce properly sized reentrant cavities should be used in order to assure the surface will perform as desired.

Although great care was taken to avoid the influence of dissolved gases, it is suspected that this also could have had an effect on the results of the four surfaces. Depending on their shapes, cavities can contain gas. Since the flow loop and the test section are not sealed off from the atmosphere, gases are free to permeate to and from the working fluid. An excess concentration of dissolved gases concentrated at the nucleation sites would make the surface seem to perform better than it normally would by inducing the premature incipience of boiling. It is expected that the effect of these dissolved gasses on the results of this experiment were small, on the order of 2-3%. Data in this work was taken with increasing heat flux, however, some more of the dissolved gas problem could have been eliminated by taking data with decreasing heat flux. It may also be noted that the steep jump in heat flux, which is a characteristic of the dissolved gas effect, was not observed in any of the experiments. The initial boiling prior to the experiments seems to have eliminated much of the problem.

### 5.3 SINTERERED SUFRACE AND HYSTERESIS

The sintered surface was supplied by UOP. It was designed for hydrocarbons, however, it was expected to produce very high heat transfer coefficient values with water as well. Figure 5.8 shows the performance of the roughest surface along with the sintered surface. These tests were conducted at a Reynolds number of 7163. In these runs data was taken with increasing heat flux and also with decreasing heat flux. This was done to determine the effects of hysteresis.

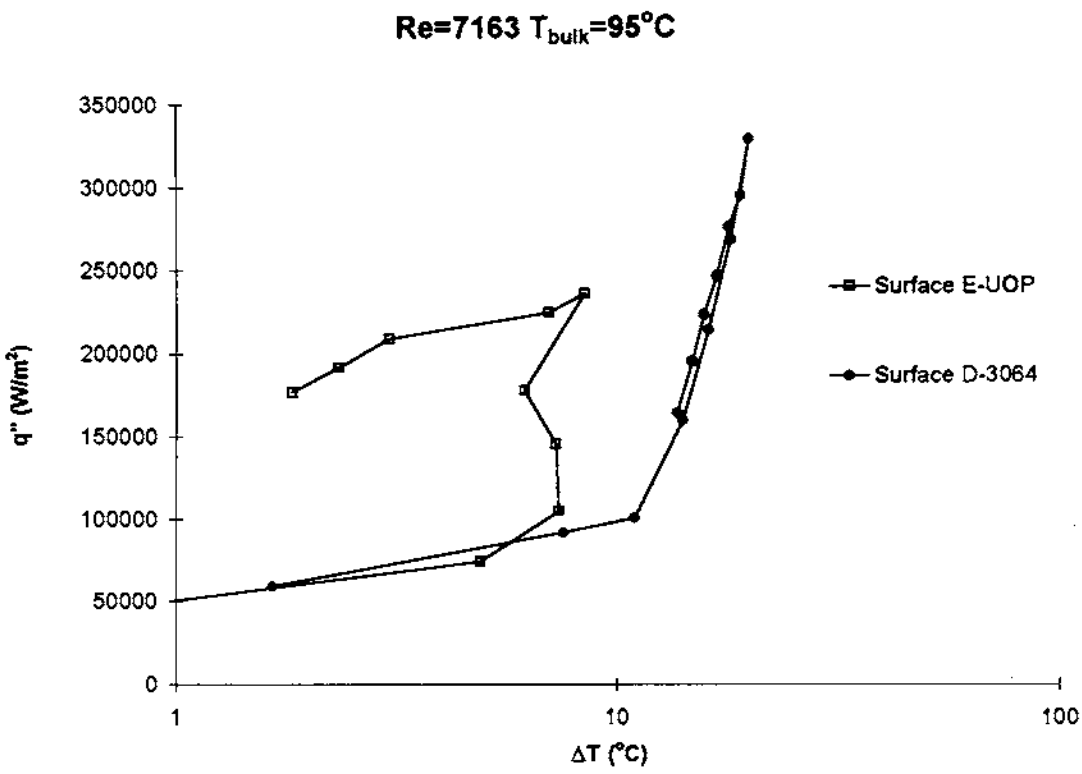


Figure 5.8 Hysteresis effects from sintered Surface E-UOP & Surface D-3064

It can be seen from the figure what a huge affect hysteresis had on the sintered surface. Both surface D-3064 and the sintered surface E-UOP exhibit a similar performance initially. The point of ONB occurs about 3-4 degrees earlier on the sintered surface though. The sintered surface really starts to out perform the plain surface as wall superheat is increased further. After reaching the highest heat flux possible , the wall superheat is decreased to study the hysteresis effect.. Surface D-3064 follows almost the exact path, exhibiting only a very

small degree of hysteresis. The sintered surface continues its enhancement all the way down sustaining boiling to only a small degree of wall superheat. It should be noted that there is some degree of uncertainty with the sintered surface heat flux data. The method used in this investigation to test the sintered surface was as follows. A tube with a sintered inside was cut down the length and flattened out. A small diameter piece was then milled out and soldered on to the existing heater surface. The contact resistance was not known exactly at this joint so its estimate may be off by up to 20%. The relative value of the heat flux from the sintered surface is still well above that of the other surfaces.

Figure 5.9 is a sketch of what the cross section of a sintered surface would look like. This sketch also shows how a saturated fluid can enter the surface as a liquid by capillary action, become vaporized, and be forced out. The size and shape of the particles used for the sintering determine the geometries of the cavities that are formed. Also varying the particle size alters the void fraction of the sintering. To optimize the surface, the sintering particle geometry should be selected depending on the working fluid and operating conditions. This will ensure that the proper size cavities are available for stable nucleation sites. For general enhancement regardless of fluid properties and working conditions, a sintering with a large number of cavities covering a wide range of sizes should be considered. Hysteresis must be accounted for when using sintering for enhancement since it can easily magnify the degree of heat transfer. It should be noted that the capillary action that is present with many sintered surfaces

helps to control fouling. The fouling agents that would be present in an industrial fluid are pushed through the surface this way. With this constant circulation a surface can help to essentially clean itself.

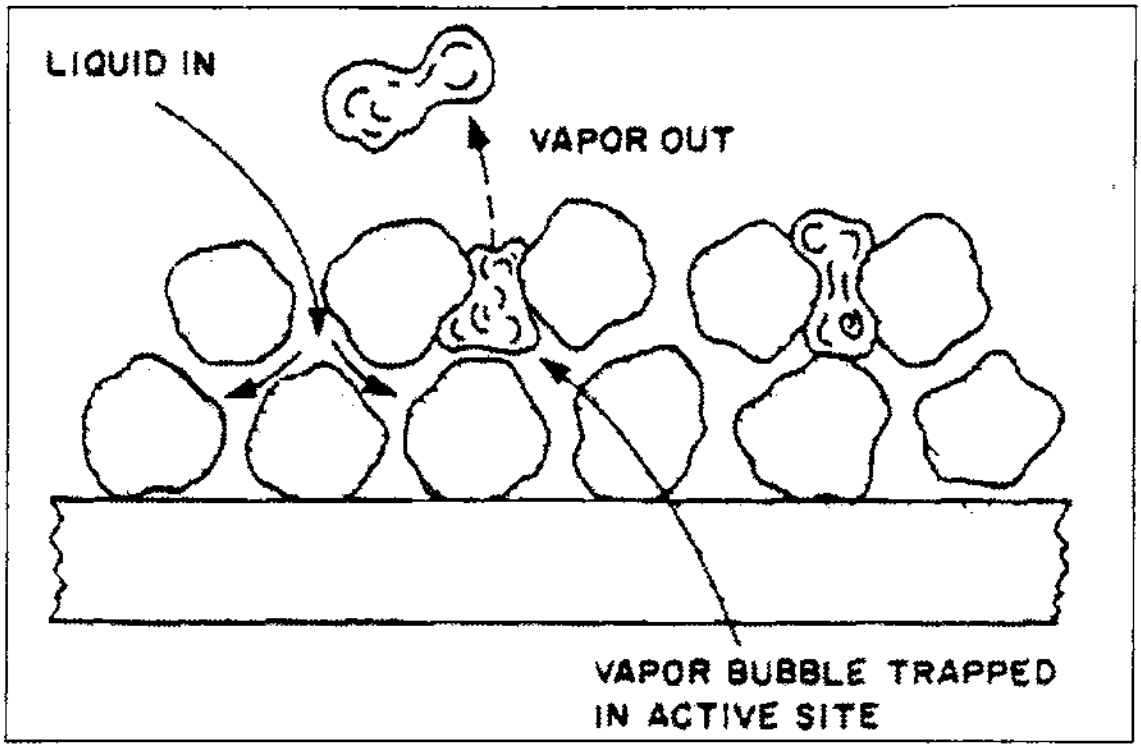


Figure 5.9 Cross Section of Sintered Surface

Adopted from Webb (1981)

# 6. CONCLUSIONS

The effect of surface characteristics on flow boiling heat transfer was evaluated experimentally with subcooled flow of water at atmospheric pressure. Four surfaces of different average surface roughness values were tested along with a sintered UOP High Flux surface in a flow boiling setup. The results were studied with respect to the cavity distributions. The following conclusions can be drawn from the present study.

- The effect of roughness was very complex but the heat transfer performance seemed to depend on the cavity size and distributions more than just the average roughness.
- A variation in the range of 0 -28.8% was found on the surfaces tested. It is expected that this "scatter" is similar to that found in flow boiling experiments reported by different investigators employing the same set of conditions.
- The active cavity range criterion was used to explain the effect of the surface roughness. The number of cavities available in the active cavity range directly relates to how many of these cavities will nucleate on a surface.
- The performance of the UOP sintered High Flux surface was considerably higher than the four roughened surfaces. This surface showed a strong hysteresis effect in comparison to one of the other four roughened surfaces.

Appropriate considerations should be made when designing boiling equipment with sintered surfaces.

- Simple surface treatments, such as sandpaper or other polishing techniques are not adequate to provide any significant improvement in heat transfer characteristics.
- Surface characteristics are an important, but not the only, parameter in determining the overall heat transfer of a surface.

There has to be a large variation in cavity geometry and size though to make large enough differences in heat transfer to be cost effective. This can be directly be related to the tubes and pipes used in industrial applications. It is recommended that this information be considered when developing enhanced surfaces for flow boiling. A sintered surface or surface with specially designed re-entrant cavities would change the surface structure enough to be effective. Air conditioning, refrigeration, nuclear, and many other industries can all benefit from enhanced surfaces. Many reboiler applications have already implemented sintered surfaces for enhancement. Sintered surfaces can show strong hysteresis effects. The hysteresis could be designed around though and the enhancement provided by the sintering is well worth the effort. It is expected that sintering will be the wave of the future in the area of heat transfer enhancement due to its possibility of order of magnitude enhancements.

# 7. SUGGESTIONS FOR FUTURE WORK

The roughness on each surface tested was obtained by using various grit sand paper. This allowed for only a random distribution of cavities. A similar setup should be employed with heater surfaces with artificially manufactured cavities. Then the cavity distribution would be known for certain since there is some uncertainty in the distributions as they are obtained in this work. Also reentrant cavities could be included. This would magnify the degree of enhancement and give more certainty to any conclusions drawn from this type of work. A second suggestion would be to conduct this type of cavity distribution work on a series of tubes each with different internal surface characteristics. The flow boiling data obtained from such an experiment would be closer to actual industry conditions. The data obtained from the current work is however, still quite valid since it can predict trends on a greater scale.

## 8. REFERENCES


Berenson, P. J., 1962, "Experiments on Pool Boiling Heat Transfer," *Int. J. Heat Mass Trans.*, Vol. 5, pp. 985-999.

Bergles, A. E., and Rohsenow, W. M., 1964, "The Determination of Forced-Convection Surface-boiling Heat Transfer," *Journal of Heat Transfer, Trans. ASME,* Series C, Vol. 86, No. 3, pp. 365-372.

Czikk, A. M., and O'Neill, P. S., 1979, "Correlation of Nucleate Boiling from Porous Metal Films," *Advances in Enhanced Heat Transfer*, ASME New York, pp. 103-113.

Howell, M., 1996, "Investigation of nucleation and heat transfer during subcooled flow boiling on augmented surfaces, " M.S. Thesis, ME Department, Rochester Institute of Tech., Rochester, N.Y.

Hsu, Y. Y., 1962, "On the Size Range of Active Nucleation Cavities on a Heating Surface," *J. Heat Transfer, Trans. ASME,* Vol. 84, pp. 207-216.

Kurihari, H. M., and Myers, J. E., 1960, "Effects of Superheat and Roughness on the Boiling Coefficients," *AIChE J.,* Vol. 6, No. 1, pp. 83-91.

Kandlikar, S.G., and Howell, M.J., "Investigation of Nucleation and Heat Transfer for Subcooled Flow Boiling on Microfin Surfaces," *2nd European Thermal-Sciences and 14th UIT National Heat Transfer Conference 1996*, Vol. 1, pp. 241-247.

Kandlikar, S. G., and Raykoff, T., 1997, "Predicting Flow Boiling Heat Transfer of Refrigerants in Microfin Tubes, Accepted for publication in the *Journal of Enhanced Heat Transfer.*

Kandlikar, S.G., and Raykoff, T., 1996, Predicting Flow Boiling Heat Transfer for Refrigerants in Plain and Microfin Tubes,@ *2nd European Thermal-Sciences and 14th UIT National Heat Transfer Conference1996*, G.P. Celata, P.Di Marco, and A. Mariani, eds., Edizioni ETS Publishers, Italy, pp. 475-482.

Kandlikar, S.G., and Spiesman, P.H., "Effect of Surface Characteristics on Flow Boiling Heat Transfer," paper presented at Convective Flow and Pool Boiling Conference, Isree, Germany, May 1997

Marto, P. J., Moulson, J. A., and Maynard, M. D., 1968, "Nucleate Pool Boiling of Nitrogen with Different Surface Conditions," *J. Heat Transfer, Trans. ASME,* Vol. 90, pp. 437-445.

Sato, T., and Matsumura, H., 1964, "On the Conditions of Incipient Subcooled Boiling with Forced Convection," *Bulletin of JSME*, Vol. 26, pp. 392-398.

Stumm, B.J., 1994, "Investigation of bubble departure in subcooled flow boiling of water," M.S. Thesis, ME Department, Rochester Institute of Tech., Rochester, N.Y.

Raykoff, T., 1996, "Bubble Growth Rate and Heat Transfer Suppression in the Flow Boiling of Binary Mixtures." M.S. Thesis, ME Department, Rochester Institute of Tech., Rochester, N.Y.

Rohsenow, W. M., 1985, Handbook of Heat Transfer, McGraw Hill Publishers, New York, N.Y.

Wadekar, V.V., "A Comparative Study of In-Tube Boiling on Plain and High Flux Coated Surfaces," 2nd European Thermal-Sciences and 14th UIT National Heat Transfer Conference 1996, Vol. 1, pp. 195-201.

Webb, R. L., 1981, "The Evolution of Enhanced Surface Geometries for Nucleate Boiling," *Heat Transfer Engineering*, Vol. 2 nos. 3-4, pp. 46-69.

Webb, R. L., 1981, "Nucleate Boiling on Porous Coated Surfaces," *Heat Transfer Engineering*, Vol. 4 nos. 3-4, pp. 71-82.

# 9. APPENDIX A SURFACE IMAGES


Figure A.1 Heater Surface D-3064, $R_a$ = 3.064 μm, 125X Magnification

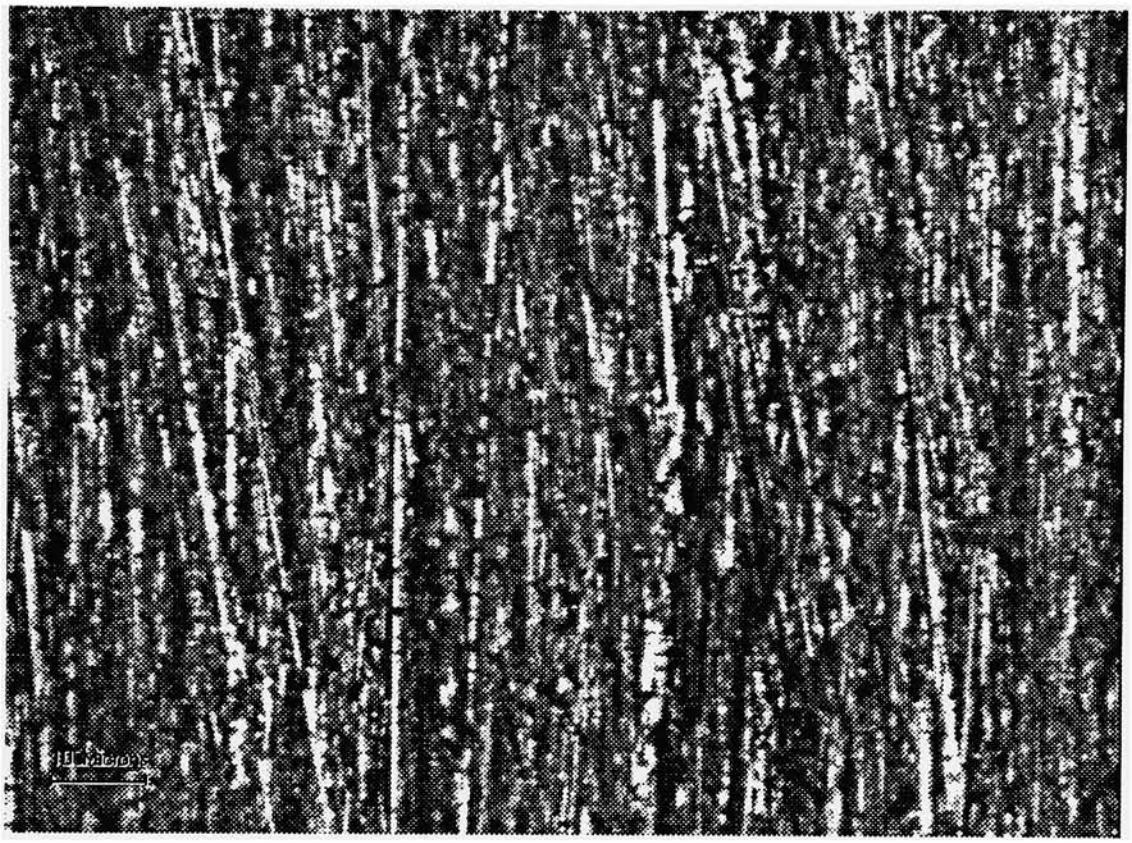

Figure A.2 Heater Surface C-716, $R_a$ = 0.716 μm, 125X Magnification

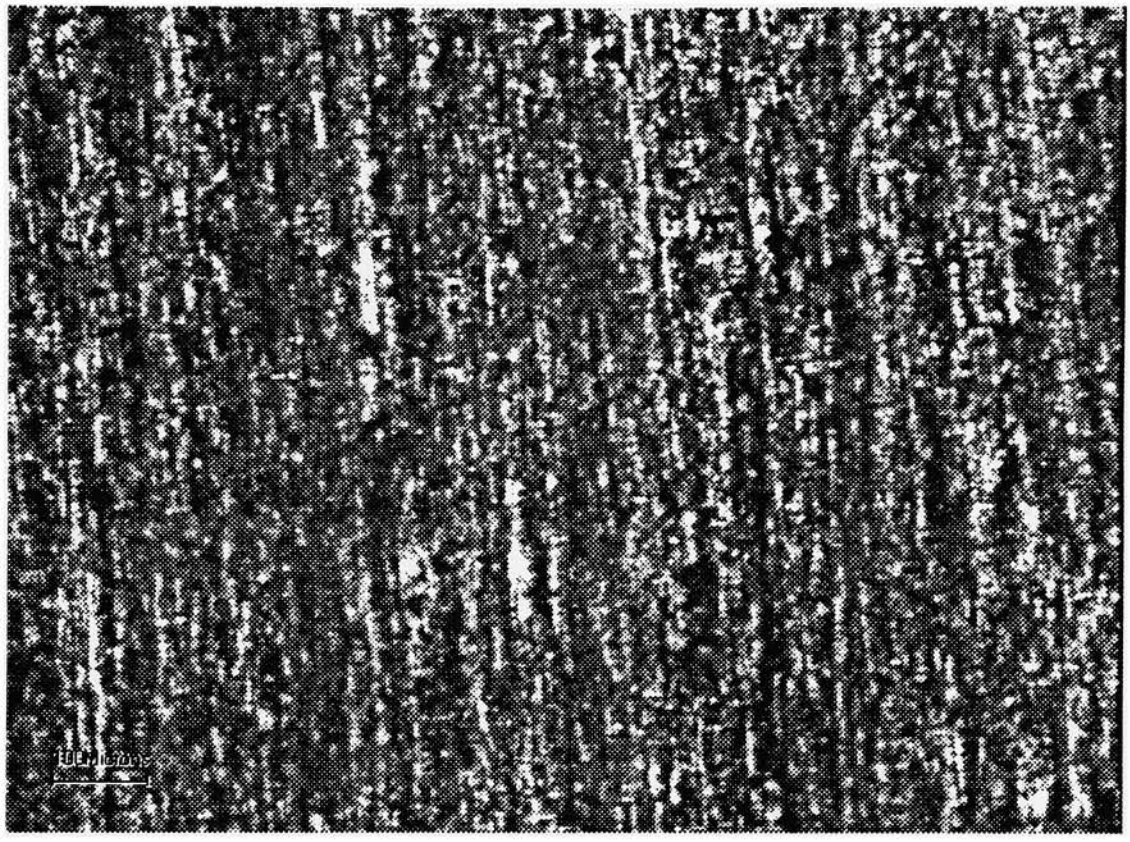

Figure A.3 Heater Surface B-363, $R_a$ = 0.363 μm, 125X Magnification

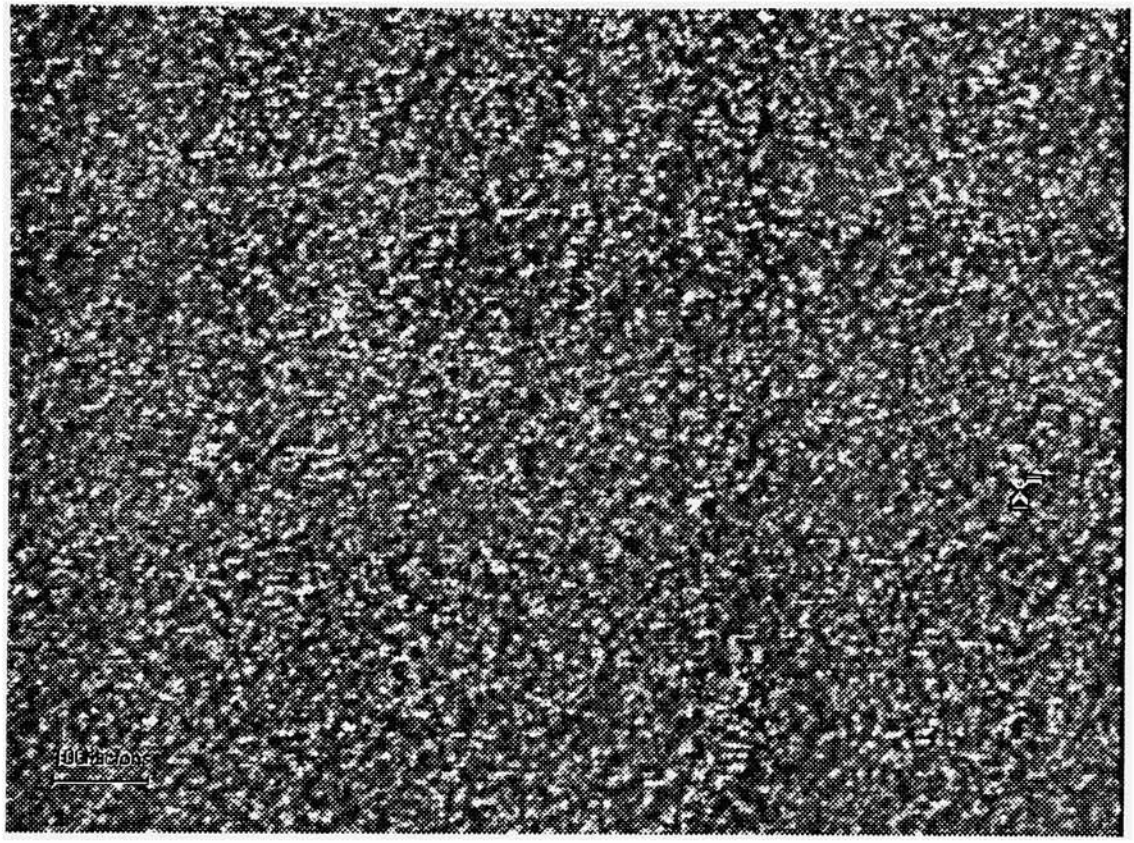

Figure A.4 Heater Surface A-188, $R_a$ = 0.188 μm, 125X Magnification

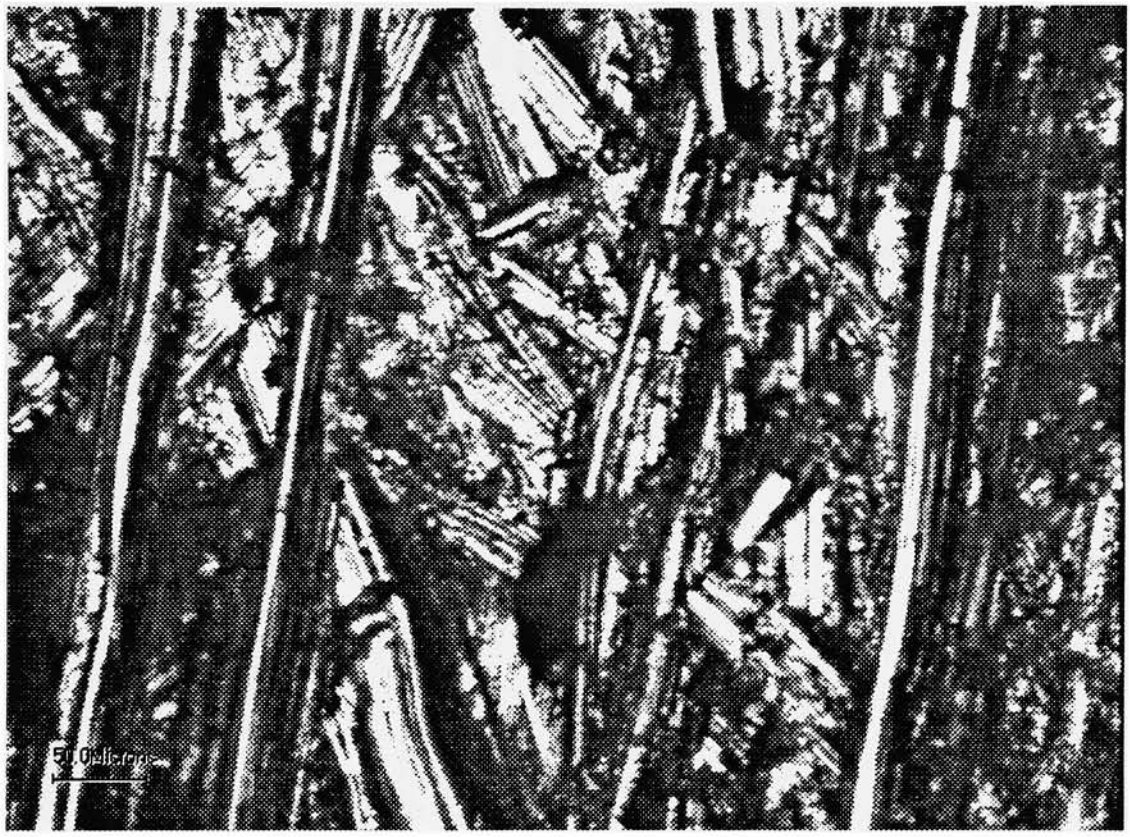

Figure A.5 Heater Surface D-3064, $R_a$ = 3.064 μm, 250X Magnification

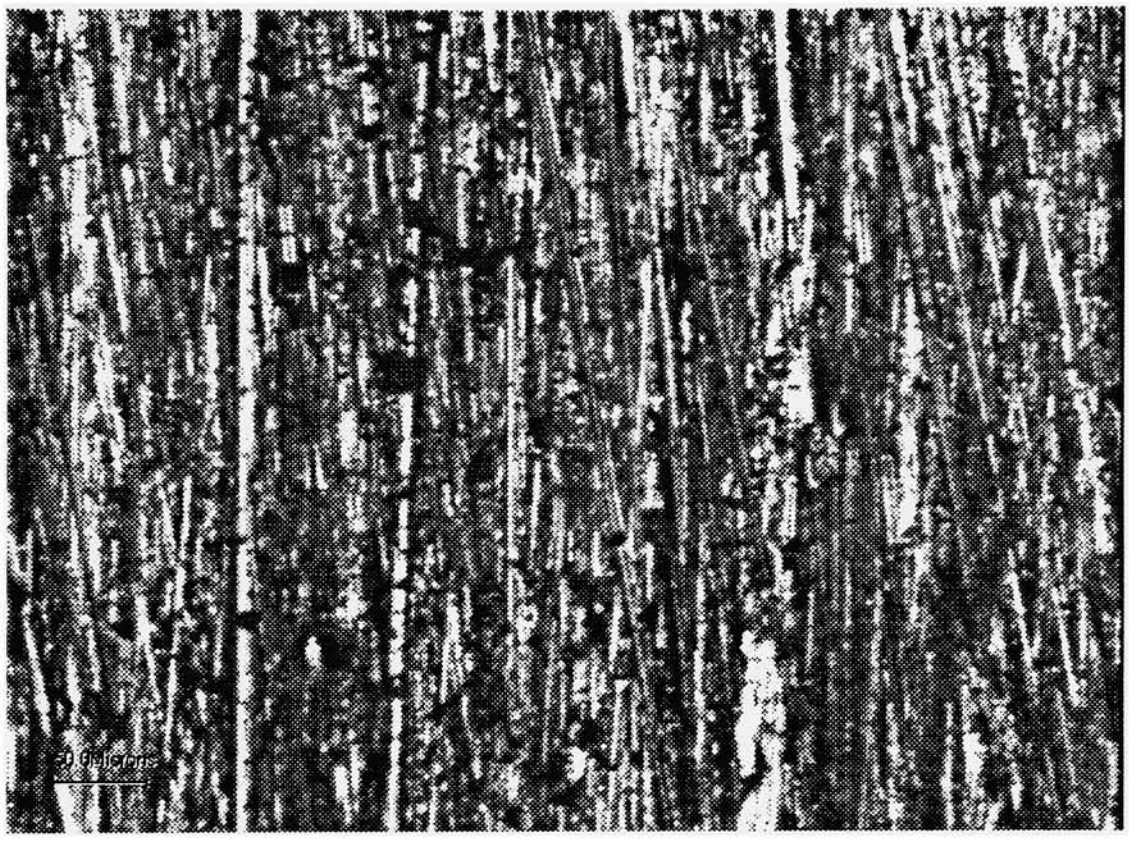

Figure A.6 Heater Surface C-716, $R_a$ = 0.716 μm, 250X Magnification

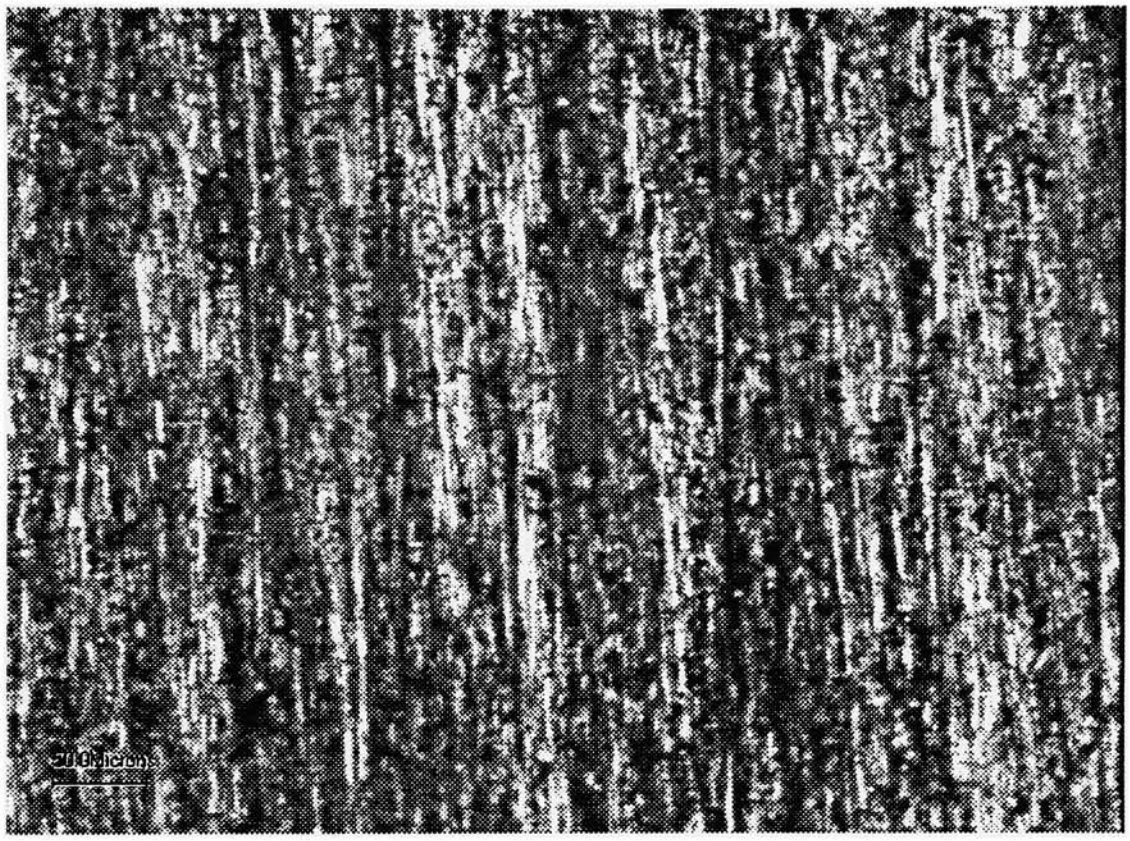

Figure A.7 Heater Surface B-363, $R_a$ = 0.363 μm, 250X Magnification

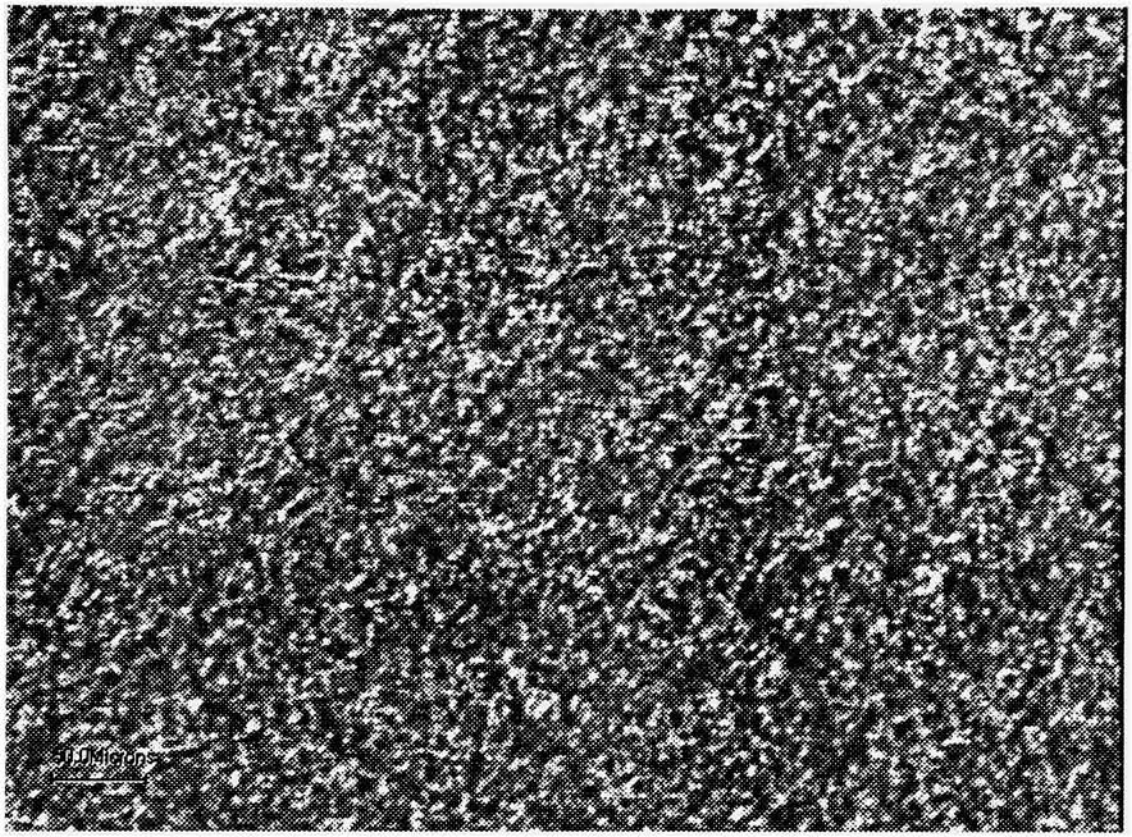


Figure A.8 Heater Surface A-188, $R_a$ = 0.188 μm, 250X Magnification

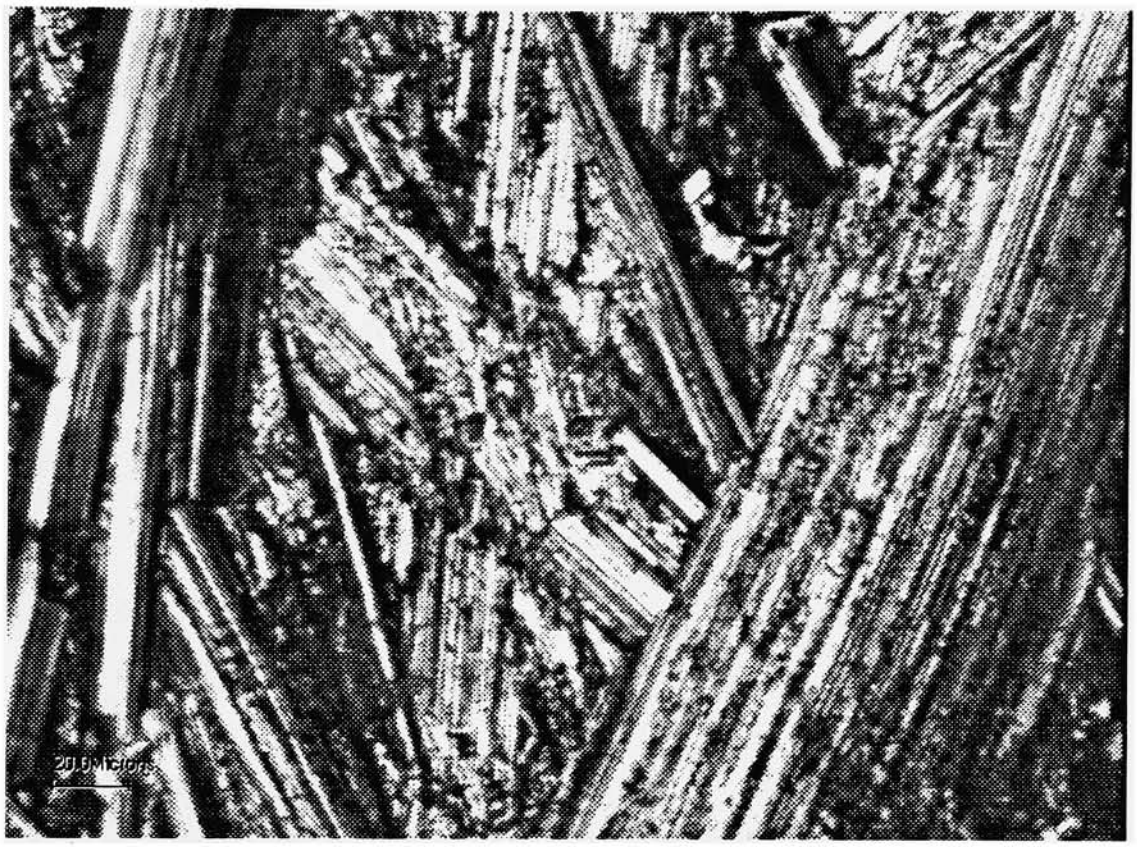

Figure A.9 Heater Surface D-3064, $R_a$ = 3.064 μm, 500X Magnification

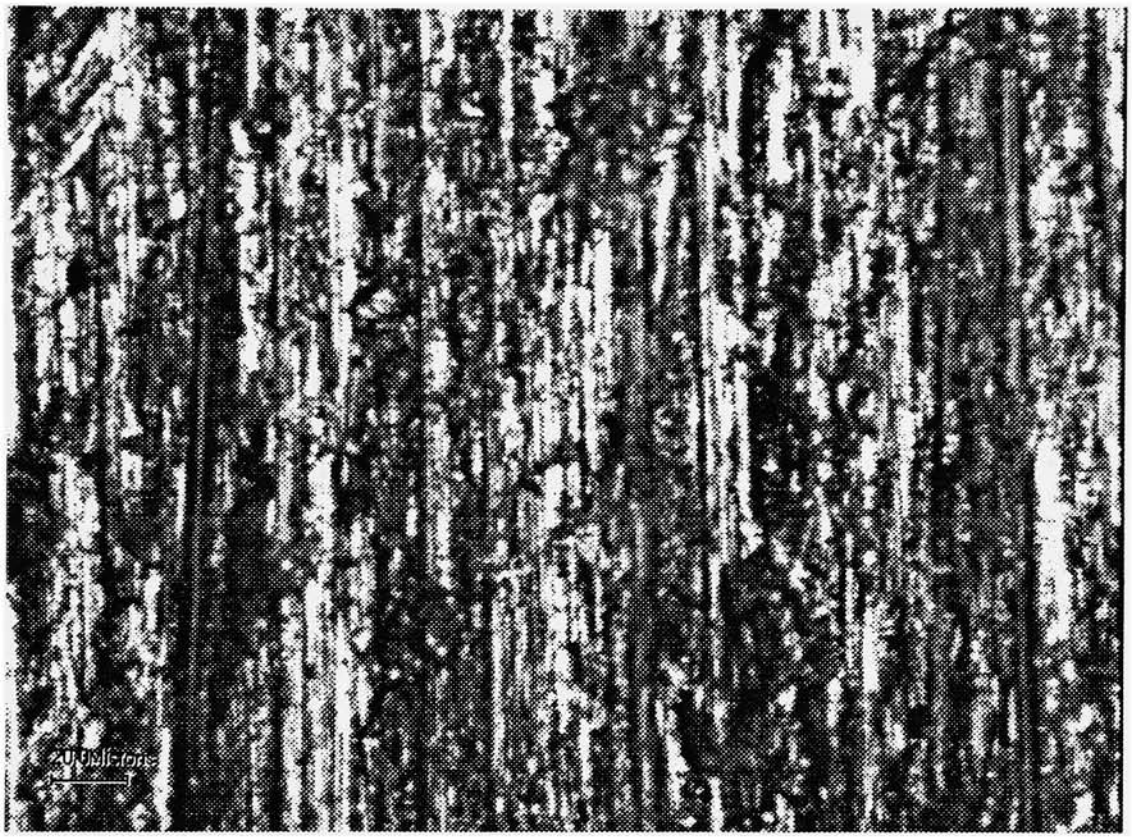

Figure A.10 Heater Surface C-716, $R_a$ = 0.716 μm, 500X Magnification

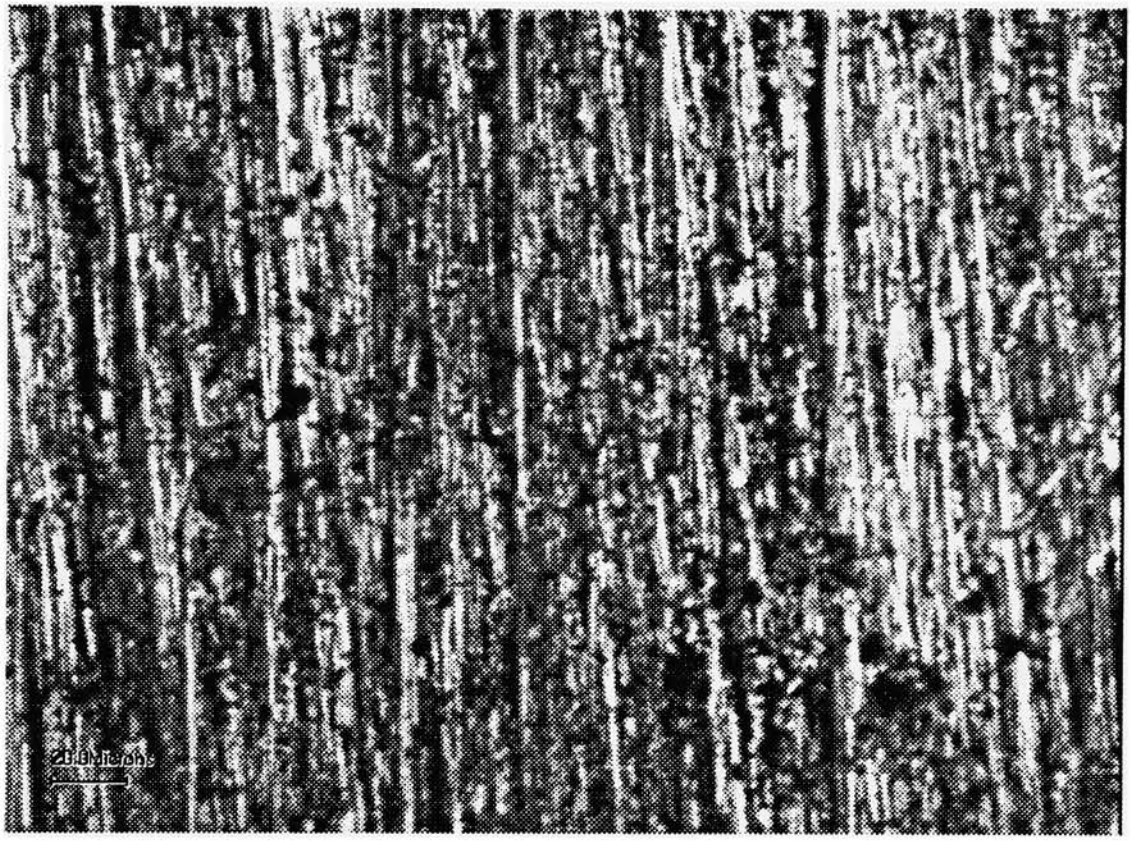

Figure A.11 Heater Surface B-363, $R_a$ = 0.363 μm, 500X Magnification

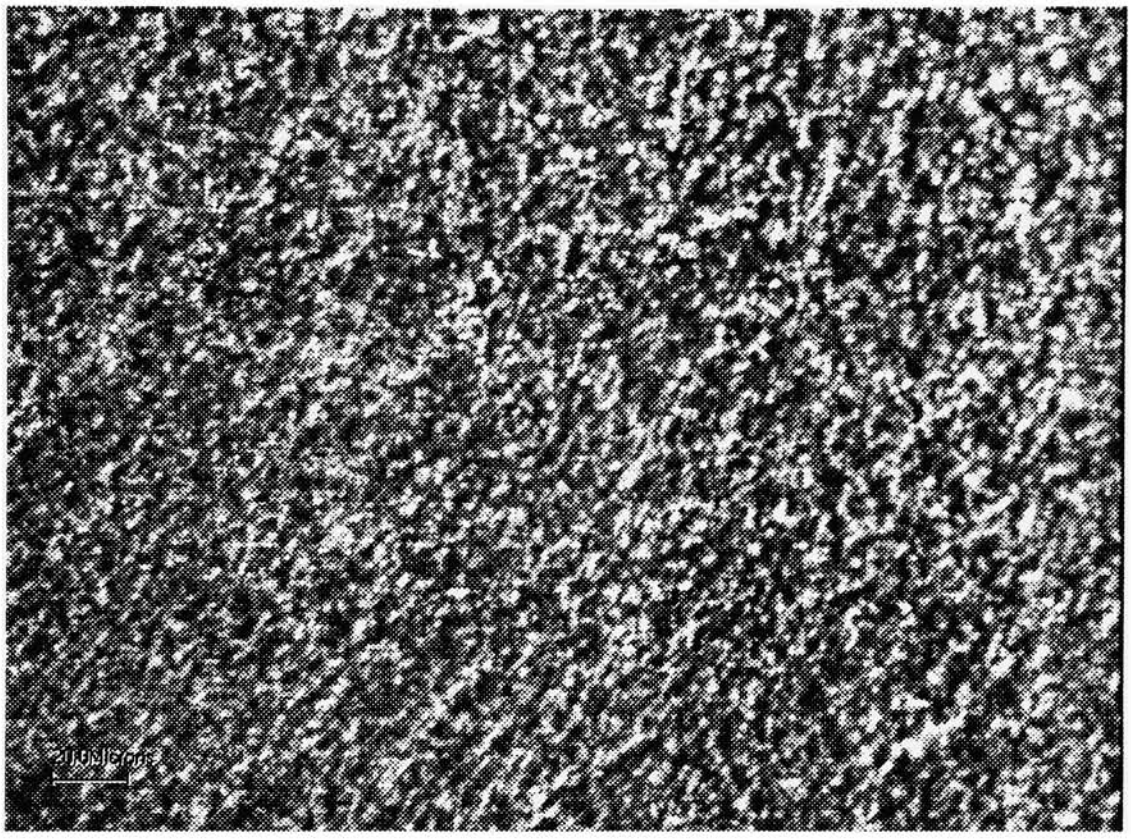

Figure A.12 Heater Surface A-188, $R_a$ = 0.188 μm, 500X Magnification

# 10. APPENDIX B DATA

| Surface | Bath Temp | Flow Rate % | Volts | Amps | T2 | T3 | T4 | T5 | T6 |
|---|---|---|---|---|---|---|---|---|---|
| 400 grit | 95 | 30 | 25 | 0.36 | 90.5 | 96.8 | 101.4 | 105.8 | 79.3 |
| 400 grit | 95 | 30 | 30 | 0.43 | 96.1 | 105.2 | 112.8 | 119.6 | 79.1 |
| 400 grit | 95 | 30 | 35 | 0.49 | 103.0 | 116.4 | 126.6 | 136.2 | 79.0 |
| 400 grit | 95 | 30 | 40 | 0.56 | 110.5 | 123.7 | 139.5 | 155.9 | 79.5 |
| 400 grit | 95 | 30 | 45 | 0.63 | 118.4 | 135.1 | 155.1 | 175.7 | 79.7 |
| 400 grit | 95 | 30 | 50 | 0.70 | 125.1 | 145.7 | 170.4 | 196.1 | 79.6 |
| 400 grit | 95 | 30 | 55 | 0.77 | 129.3 | 154.4 | 184.3 | 215.1 | 79.6 |
| 400 grit | 95 | 10 | 20 | 0.29 | 96.4 | 98.2 | 100.4 | 102.8 | 88.1 |
| 400 grit | 95 | 10 | 25 | 0.36 | 103.6 | 107.2 | 111.7 | 116.6 | 88.1 |
| 400 grit | 95 | 10 | 30 | 0.43 | 112.1 | 118.0 | 125.3 | 132.6 | 88.2 |
| 400 grit | 95 | 10 | 35 | 0.49 | 119.0 | 128.1 | 139.1 | 150.1 | 88.4 |
| 400 grit | 95 | 10 | 40 | 0.56 | 121.8 | 134.1 | 148.8 | 163.6 | 89.2 |
| 400 grit | 95 | 10 | 45 | 0.63 | 123.9 | 140.3 | 159.7 | 179.8 | 89.3 |
| 400 grit | 95 | 10 | 50 | 0.70 | 126.0 | 146.4 | 170.5 | - | 89.3 |
| 400 grit | 95 | 10 | 55 | 0.77 | 128.6 | 154.4 | 185.1 | - | 89.4 |
| 600 grit | 95 | 30 | 20 | 0.29 | 98.6 | 100.5 | 102.6 | 105.2 | 93.9 |
| 600 grit | 95 | 30 | 25 | 0.36 | 102.9 | 106.8 | 111.6 | 116.8 | 93.6 |
| 600 grit | 95 | 30 | 30 | 0.43 | 107.8 | 114.1 | 121.6 | 129.7 | 93.7 |
| 600 grit | 95 | 30 | 35 | 0.49 | 113.5 | 123.1 | 134.2 | 146.2 | 93.8 |
| 600 grit | 95 | 30 | 40 | 0.56 | 119.3 | 132.0 | 147.1 | 163.2 | 93.9 |
| 600 grit | 95 | 30 | 45 | 0.63 | 123.2 | 139.8 | 159.5 | 180.3 | 94.0 |
| 600 grit | 95 | 30 | 50 | 0.70 | 125.6 | 146.6 | 171.5 | - | 94.1 |
| 600 grit | 95 | 30 | 55 | 0.77 | 128.5 | 154.0 | 184.2 | - | 94.1 |
| 600 grit | 95 | 10 | 20 | 0.29 | 95.1 | 96.7 | 98.6 | 100.9 | 88.0 |
| 600 grit | 95 | 10 | 25 | 0.36 | 103.0 | 106.7 | 111.0 | 115.9 | 88.9 |
| 600 grit | 95 | 10 | 30 | 0.43 | 110.3 | 116.1 | 123.0 | 130.6 | 89.1 |
| 600 grit | 95 | 10 | 35 | 0.49 | 117.2 | 126.2 | 137.0 | 148.6 | 89.2 |
| 600 grit | 95 | 10 | 40 | 0.56 | 120.1 | 132.3 | 147.1 | 163.0 | 89.3 |
| 600 grit | 95 | 10 | 45 | 0.63 | 122.4 | 138.9 | 158.6 | 179.5 | 89.6 |
| 600 grit | 95 | 10 | 50 | 0.70 | 124.5 | 145.3 | 170.2 | 195.8 | 89.6 |
| 600 grit | 95 | 10 | 55 | 0.77 | 126.6 | 151.9 | 182.1 | 213.1 | 89.6 |
| 120 grit | 95 | 10 | 20 | 0.29 | 98.4 | 100.4 | 102.9 | 105.7 | 89.6 |
| 120 grit | 95 | 10 | 25 | 0.36 | 105.1 | 108.8 | 113.5 | 118.7 | 89.5 |
| 120 grit | 95 | 10 | 30 | 0.43 | 113.8 | 120.1 | 127.8 | 136.1 | 89.6 |
| 120 grit | 95 | 10 | 35 | 0.49 | 117.1 | 126.8 | 138.7 | 151.2 | 89.5 |
| 120 grit | 95 | 10 | 40 | 0.56 | 119.2 | 132.5 | 148.6 | 165.5 | 89.8 |
| 120 grit | 95 | 10 | 45 | 0.63 | 121.2 | 138.6 | 159.4 | 181.1 | 89.8 |
| 120 grit | 95 | 10 | 50 | 0.70 | 123.7 | 145.5 | 171.6 | 198.7 | 90.0 |
| 120 grit | 95 | 10 | 55 | 0.77 | 126.2 | 152.8 | 184.5 | 217.4 | 90.4 |
| 120 grit | 95 | 30 | 20 | 0.29 | 101.1 | 103.9 | 107.3 | 111.1 | 93.7 |
| 120 grit | 95 | 30 | 25 | 0.36 | 104.2 | 108.4 | 113.5 | 119.0 | 93.8 |
| 120 grit | 95 | 30 | 30 | 0.43 | 110.4 | 117.2 | 125.5 | 134.3 | 93.8 |
| 120 grit | 95 | 30 | 35 | 0.49 | 115.6 | 125.4 | 137.3 | 149.9 | 93.9 |
| 120 grit | 95 | 30 | 40 | 0.56 | 118.8 | 132.2 | 148.4 | 165.3 | 94.1 |
| 120 grit | 95 | 30 | 45 | 0.63 | 121.4 | 139.5 | 161.1 | 183.6 | 94.2 |
| 120 grit | 95 | 30 | 50 | 0.70 | 123.8 | 145.9 | 172.1 | 199.4 | 94.2 |
| 120 grit | 95 | 30 | 55 | 0.77 | 126.3 | 152.7 | 184.3 | 216.8 | 94.3 |

| Surface | Bath Temp | Flow Rate % | Volts | Amps | T2 | T3 | T4 | T5 | T6 |
|---|---|---|---|---|---|---|---|---|---|
| polished | 95 | 30 | 20 | 0.29 | 99.0 | 101.1 | 103.6 | 106.4 | 93.7 |
| polished | 95 | 30 | 25 | 0.36 | 103.6 | 107.7 | 112.8 | 118.3 | 93.5 |
| polished | 95 | 30 | 30 | 0.43 | 108.8 | 115.5 | 123.7 | 132.3 | 93.7 |
| polished | 95 | 30 | 35 | 0.49 | 112.9 | 122.9 | 134.8 | 147.4 | 93.8 |
| polished | 95 | 30 | 40 | 0.56 | 118.1 | 131.2 | 147.2 | 163.9 | 93.8 |
| polished | 95 | 30 | 45 | 0.63 | 121.1 | 138.8 | 159.8 | 181.7 | 94.0 |
| polished | 95 | 30 | 50 | 0.70 | 123.9 | 145.7 | 171.8 | 198.9 | 94.0 |
| polished | 95 | 30 | 55 | 0.77 | 126.0 | 152.9 | 184.8 | 217.9 | 93.8 |
| polished | 95 | 10 | 20 | 0.29 | 96.2 | 98.1 | 100.3 | 112.8 | 88.4 |
| polished | 95 | 10 | 25 | 0.36 | 104.4 | 108.2 | 112.9 | 117.9 | 89.7 |
| polished | 95 | 10 | 30 | 0.43 | 113.2 | 119.4 | 126.9 | 135.0 | 89.6 |
| polished | 95 | 10 | 35 | 0.49 | 117.9 | 127.3 | 138.8 | 150.9 | 89.5 |
| polished | 95 | 10 | 40 | 0.56 | 120.5 | 133.5 | 149.2 | 165.7 | 89.6 |
| polished | 95 | 10 | 45 | 0.63 | 122.6 | 139.8 | 160.5 | 182.0 | 89.6 |
| polished | 95 | 10 | 50 | 0.70 | 124.8 | 146.4 | 172.5 | 199.5 | 90.2 |
| polished | 95 | 10 | 55 | 0.77 | 127.4 | 153.8 | 185.4 | 218.1 | 90.3 |
| sintered | 95 | 30 | 20 | 0.29 | 105.2 | 106.2 | 108.0 | 110.0 | 93.9 |
| sintered | 95 | 30 | 25 | 0.36 | 115.0 | 117.1 | 120.5 | 124.3 | 93.8 |
| sintered | 95 | 30 | 30 | 0.43 | 129.4 | 133.0 | 138.9 | 145.4 | 93.9 |
| sintered | 95 | 30 | 35 | 0.49 | 142.0 | 147.1 | 155.5 | 164.7 | 93.9 |
| sintered | 95 | 30 | 40 | 0.56 | 156.7 | 163.9 | 175.5 | 188.2 | 94.0 |
| sintered | 95 | 30 | 45 | 0.63 | 165.3 | 174.0 | 188.3 | 203.8 | 94.0 |
| sintered | 95 | 30 | 50 | 0.70 | 187.0 | 198.6 | 217.8 | 238.1 | 94.2 |
| sintered | 95 | 30 | 48 | 0.67 | 181.3 | 192.3 | 210.6 | 229.9 | 94.2 |
| sintered | 95 | 30 | 46 | 0.64 | 172.9 | 183.2 | 200.2 | 218.0 | 94.2 |
| sintered | 95 | 30 | 44 | 0.62 | 165.9 | 175.3 | 190.9 | 207.3 | 94.2 |
| sintered | 95 | 30 | 42 | 0.59 | 159.5 | 168.1 | 182.6 | 197.7 | 94.1 |
| sintered | 95 | 30 | 40 | 0.56 | 153.1 | 160.9 | 173.9 | 187.7 | 93.9 |
| sintered | 95 | 30 | 38 | 0.53 | 147.8 | 154.9 | 166.7 | 179.2 | 94.0 |
| sintered | 95 | 30 | 36 | 0.51 | 142.2 | 148.5 | 158.9 | 169.9 | 93.9 |
| sintered | 95 | 30 | 34 | 0.48 | 136.3 | 141.8 | 150.9 | 160.6 | 93.8 |
| sintered | 95 | 30 | 32 | 0.45 | 131.0 | 135.8 | 143.6 | 151.9 | 93.8 |
| sintered | 95 | 30 | 30 | 0.42 | 126.3 | 130.3 | 136.9 | 144.0 | 93.8 |
| sintered | 95 | 30 | 28 | 0.40 | 122.2 | 125.6 | 131.2 | 137.2 | 93.7 |
| sintered | 95 | 30 | 26 | 0.37 | 118.4 | 121.3 | 126.0 | 131.2 | 93.7 |
| sintered | 95 | 30 | 24 | 0.34 | 113.4 | 115.7 | 119.5 | 123.7 | 93.7 |
| sintered | 95 | 30 | 22 | 0.31 | 109.7 | 111.5 | 114.6 | 117.9 | 93.6 |
| 120 grit | 95 | 30 | 20 | 0.29 | 102.8 | 106.6 | 110.1 | 121.2 | 89.2 |
| 120 grit | 95 | 30 | 25 | 0.36 | 108.7 | 114.6 | 118.5 | 135.4 | 89.7 |
| 120 grit | 95 | 30 | 30 | 0.43 | 112.9 | 119.4 | 129.9 | 141.5 | 89.9 |
| 120 grit | 95 | 30 | 35 | 0.49 | 117.2 | 127.5 | 143.9 | 161.7 | 90.0 |
| 120 grit | 95 | 30 | 40 | 0.56 | 120.3 | 134.1 | 156.0 | 179.6 | 90.5 |
| 120 grit | 95 | 30 | 45 | 0.63 | 123.3 | 140.6 | 167.8 | 196.9 | 90.6 |
| 120 grit | 95 | 30 | 50 | 0.70 | 126.2 | 147.4 | 180.8 | 216.0 | 90.5 |
| 120 grit | 95 | 30 | 55 | 0.77 | 124.7 | 143.7 | 173.7 | 205.4 | 90.6 |
| 120 grit | 95 | 30 | 52 | 0.73 | 123.2 | 141.0 | 166.6 | 195.0 | 90.5 |
| 120 grit | 95 | 30 | 49 | 0.68 | 121.6 | 137.5 | 159.8 | 184.8 | 90.4 |
| 120 grit | 95 | 30 | 46 | 0.64 | 120.1 | 134.5 | 153.2 | 175.3 | 90.3 |
| 120 grit | 95 | 30 | 43 | 0.60 | 118.6 | 131.2 | 147.6 | 166.8 | 90.3 |
| 120 grit | 95 | 30 | 40 | 0.56 | 116.9 | 127.5 | 141.3 | 157.5 | 90.1 |

## 11. APPENDIX C REYNOLDS NUMBER CALCULATIONS

The Reynolds number is calculated by using the following equation:

$$Re = \frac{\rho v d_H}{\mu} \qquad (C.1)$$

where $d_H$ is the hydraulic diameter calculated by:

$$d_H = \frac{4A_c}{P_w} \qquad (C.2)$$

$A_c$ is the cross sectional area of the test section and $P_w$ is the wetted perimeter of the test section.

The velocity of the fluid v is calculated as follows:

$$v = \frac{volumeicflow}{A_c} \qquad (C.3)$$

where the volumetric flow is taken as a % of the maximum volumetric flow of 2.53 GPM.

Properties were taken at bulk liquid temperatures.